Thermophysical properties of carbon–argon and carbon–helium plasmas

2011 J. Phys. D: Appl. Phys. 44 355207

(http://iopscience.iop.org/0022-3727/44/35/355207)

IOP PUBLISHING JOURNAL OF PHYSICS D: APPLIED PHYSICS

J. Phys. D: Appl. Phys. **44** (2011) 355207 (18pp) doi:10.1088/0022-3727/44/35/355207

Thermophysical properties of carbon–argon and carbon–helium plasmas

WeiZong Wang[1,2], MingZhe Rong[1], Anthony B Murphy[3], Yi Wu[1], Joseph W Spencer[2], Joseph D Yan[2] and Michael T C Fang[2]

[1] State Key Laboratory of Electrical Insulation and Power Equipment, Xi'an Jiaotong University, Xi'an Shaanxi 710049, People's Republic of China
[2] Department of Electrical Engineering and Electronics, The University of Liverpool, Brownlow Hill, Liverpool L69 3GJ, UK
[3] CSIRO Materials Science and Engineering, PO Box 218, Lindfield NSW 2070, Australia

E-mail: mzrong@mail.xjtu.edu.cn

Received 21 April 2011, in final form 11 July 2011
Published 18 August 2011
Online at stacks.iop.org/JPhysD/44/355207

Abstract
The calculated values of thermodynamic and transport properties of mixtures of carbon and argon, and carbon and helium, at high temperatures are presented in this paper. The thermodynamic properties are determined by the method of Gibbs free energy minimization, using standard thermodynamic tables. The transport properties including electron diffusion coefficients, viscosity, thermal conductivity and electrical conductivity are evaluated using the Chapman–Enskog method expanded up to the third-order approximation (second order for viscosity). Collision integrals are obtained using the most accurate cross-section data that could be located. The calculations, which assume local thermodynamic equilibrium, are performed for atmospheric pressure plasmas in the temperature range from 300 to 30 000 K for different pressures between 0.1 and 10 atm. The results are compared with those of previously published studies. Good agreement is found for pure argon and helium. Larger discrepancies occur for carbon and mixtures of carbon and argon, and carbon and helium; these are explained in terms of the different values of the collision integrals that were used. The results presented here are expected to be more accurate because of the improved collision integrals employed.

(Some figures in this article are in colour only in the electronic version)

1. Introduction

Carbon nanostructures and nanomaterials, including carbon nanotubes, fullerenes and graphene, have generated a huge amount of interest, because of their unique properties and their wide range of potential applications [1]. Fullerenes, molecules composed entirely of carbon and taking the form of a hollow sphere, ellipsoid, tube or ring, were discovered in 1980 [2]. Their exceptional physical properties and their potential applications as optical materials, as superconductors, in reinforced polymers and in other biological and medical applications have raised a great deal of interest in the recent scientific literature [3–7].

Carbon nanotubes are close cousins of fullerenes in terms of production method and some of their properties. Since they were first found using the Kratschmer–Huffman carbon arc method in 1991 [8] and the modifications developed by Dravid *et al* [9], they too have attracted broad attention. Their novel properties make them potentially useful in many applications in nanotechnology, electronics, optics and other fields of materials science, as well as potential uses in architectural fields [10–16].

Graphene, a one-atom-thick sheet of carbon atoms, was discovered using a mechanical method in 2004 [17]. It exhibits remarkable properties, including quantum Hall effect at room temperature, ballistic conduction and a tunable band gap.

Potential applications include as field emitters, in composite materials, in field-effect transistors and in ultrasensitive sensors [18].

Large-scale high-rate preparation of high-purity fullerenes and other carbon nanomaterials is a prerequisite for the observation of their structure, performance testing, further research and practical applications. One of the main candidates for such production is the arc discharge process, using graphite electrodes in the reaction chamber into which an inert gas such as argon or helium atmosphere is supplied [19–25] .The typical pressure range used is from 0.1 to 1 atm. Shi *et al* increased the pressure to 2 atm and found that high helium pressure can lead to a high yield of single-wall carbon nanotubes, indicating the potential of using higher pressures in the future [26].

Carbon–argon and carbon–helium mixtures are also widely used in other industrial arc and plasma processes. For example, a new powder surfacing process using a carbon-electrode arc shielded by argon was investigated and found to give improved alloy transfer and surface properties [27].

Modelling of processes such as those mentioned above can assist in optimization of process design, as well as give a better understanding of the phenomena involved [28, 29]. Of particular note is that accurate data for the composition, thermodynamic properties and transport coefficients are a prerequisite for reliable numerical simulation of thermal plasmas. Unfortunately, transport coefficients are difficult to calculate, and large discrepancies remain in the values presented by different authors. These partly result from the uncertainties in the gas composition and approximations made in the calculations, but are mainly due to uncertainties in the values of the intermolecular potentials from which the transport coefficients are derived [30].

We know of no experimental study and only one theoretical paper, that of Pousse *et al* [31], in which the thermophysical properties of carbon–argon and carbon–helium mixtures are presented. Pousse *et al* specifically investigated mixtures for fullerene synthesis in the pressure range from 0.1 to 1 atm and for temperatures from 300 to 20 000 K. They neglected the presence of solid carbon, and the associated phase transition, at low temperatures. The input data used, such as the intermolecular potentials, were adequate representations over limited temperature ranges. However, much relevant experimental and theoretical work has been performed since that time and more accurate representations of the intermolecular potentials, which can reduce the uncertainties in the values of transport coefficients, are available for many interactions relevant to carbon–argon and carbon–helium mixtures.

This paper assumes that the plasmas are in local thermodynamic equilibrium (LTE) and uses the best available data to obtain a more reliable calculation of the species composition, thermodynamic properties and transport coefficients of pure carbon, carbon–argon and carbon–helium mixtures for the extended temperature range 300–30 000 K and a wide pressure range 0.10–10 atm, conditions which satisfy most thermal plasma modelling requirements. Compared with previous work, results determined by more reliable data are presented both including and neglecting the presence of solid carbon at low temperatures. The validity of the results is confirmed through comparison with published results for pure helium and argon, which have been studied by many authors and can be regarded as benchmark systems.

This paper includes the following sections:

(1) Details of the computational technique for the determination of composition and thermodynamic properties.
(2) A discussion of the methods used to calculate the transport coefficients.
(3) The collision integrals, the choice of intermolecular potentials used in evaluating them and various approaches used in determining transport properties.
(4) Calculated compositions, thermodynamic data and transport coefficients, and a comparison of the calculated properties with available data in the literature.

2. Determination of composition and thermodynamic properties

A prerequisite to obtaining thermodynamic properties and transport coefficients of mixtures is the determination of the species composition [32]. The calculations are based on the conservation of the elements, Dalton's law, the law of mass action (Saha's law and Gulberg–Waage's law) and electrical quasi-neutrality [33]. The chemical equilibrium composition was calculated as a function of temperature and pressure based on the method of minimizing the Gibbs energy of a system [34], which is a standard technique in equilibrium chemistry [35]. A descent Newton–Raphson iteration method was used to solve the nonlinear equations which are related to the fundamental law expressions mentioned above. The Debye–Hückel correction was taken into account and applied to the chemical potential of charged species, and to the total number density of the plasma, as described by Kovitya [36]. The required thermodynamic data for neutral atoms and positively charged atomic ions were calculated from the internal partition functions, which were derived from the energy level tabulated by Moore [37, 38]. Data for other species were taken from the JANAF Thermochemical Tables in the form of polynomials whose coefficients were fitted using a least-squares method [39] and extended to higher temperature by means of the formulae and the molecular data given with the tables.

Thermodynamic properties, such as enthalpy and specific heat, can be determined relatively simply once the composition is known, using the mass, enthalpy and number density of each species present. The mass density and the enthalpy were directly obtained from the composition of the mixture, and the specific heat at constant pressure was calculated as a numerical derivative of the enthalpy. The detailed expressions for these physical quantities can be found in [33].

For the range of temperatures and pressures considered in this paper, the relevant species are He, He^+, He^{2+} for helium, Ar, Ar^+, Ar^{2+}, Ar^{3+} for argon, and C, C_2, C_3, C_4, C_5, C^+, C^{2+}, C^{3+}, C^-, C_2^+, C_2^- for carbon, in addition to electrons. Moreover, unlike the previous paper in which condensed carbon was neglected [31], we present calculations both including and excluding solid carbon C(s). Note that other carbon particles such as clusters will form at temperatures below 2500 K;

however, they have negligible influence on the properties since most carbon is condensed at the these temperatures, and hence they are neglected in this paper.

3. Determination of transport properties

Transport properties, namely diffusion coefficients, electrical conductivity, thermal conductivities and viscosity, are calculated using the classical Chapman–Enskog method, which has been analysed comprehensively in the literature [40–42]. The distribution function of the different species is assumed to be the Maxwellian distribution function perturbed by a first-order perturbation function. The latter is developed in terms of a series of Sonine polynomials and then expressed by means of the expansion coefficients, bringing about a linearization of the Boltzmann equation and introducing systems of linear equations.

The solution of these linear equations to a selected order of approximation allows one to obtain transport coefficients. The order chosen in the calculation determines the dimensions of the system of linear equations with which the distribution function and the Boltzmann equation are solved with an approximate expansion expression. The accuracy of the transport properties is improved by increasing the order. However, this requires a greater number of effective collision integrals, which are terms appearing in the expressions of the transport coefficients, and the number of calculations rapidly becomes prohibitive. It has been found that at least a third-order approximation is needed at low temperatures around 5000 K for the ordinary diffusion for interactions involving electrons [43]. The first-order approximation for viscosity, as was used by Pousse *et al* [31], can differ by more than 10% at a high temperature from the third-order approximation [44]. It was concluded that in this case the second-order approximation was adequate [45]. Therefore, this paper uses the third-order approximation for transport properties except viscosity, for which the second-order approximation is considered.

For the thermal conductivity, in addition to the translational component, the contributions from the internal energy and chemical reactions should also be considered. Chemical reactions (dissociation, ionization and so on) in a plasma in chemical equilibrium results in additional heat transfer. This introduces an additional reactive thermal conductivity λ_{re}, which was studied by Butler and Brokaw for neutral gas mixtures [46]; their expressions were subsequently extended to ionized gases by Meador and Stanton [47]. The presence of internal degrees of freedom can affect the heat flux vector and is included using an internal thermal conductivity λ_{in}, which has been derived using the Hirschfelder–Eucken approximation [48–50].

4. Collision integrals

The transport coefficients rely on collision integrals which take into account the interaction potential between two species i and j. They are statistical averages over a Maxwellian distribution of the collision cross-sections for pairs of species and are defined as follows:

$$\Omega_{ij}^{(l,s)} = \sqrt{\frac{kT}{2\pi\mu_{ij}}} \int_0^\infty \exp(-\gamma_{ij}^2)\gamma_{ij}^{2s+3} Q_{ij}^l(g)\,\mathrm{d}\gamma_{ij} \quad (1)$$

where k is Boltzmann's constant, T is the temperature, μ_{ij} is the reduced mass and γ_{ij} is the reduced initial speed of the species i and j, given by

$$\gamma_{ij} = \sqrt{\frac{\mu_{ij}}{2kT}} g_{ij} \quad (2)$$

where g_{ij} is the initial relative speed of the species, and the transport cross-sections $Q_{ij}^l(g)$ are defined by

$$Q_{ij}^l(g) = 2\pi \int_0^\infty (1 - \cos^l \chi) b\,\mathrm{d}b. \quad (3)$$

The parameters χ and b are, respectively, the angle by which the molecules are deflected at the centre of the gravity coordinate system and the impact parameter of the colliding molecules i and j.

4.1. Neutral–neutral interactions

The He–He interaction was described by an accurate new potential determined from an *ab initio* calculation by Hurly [51]; the potential combines repulsive and attractive components and includes the diagonal correction to the Born–Oppenheimer model. The potential shows close agreement to measurements, and is considered to serve as a standard for the measurement of thermophysical properties. The collision integrals determined from this potential are almost identical to those calculated from the potential of Aziz *et al* [52], which has been used in the previous calculations of helium transport coefficients [30]. Note that Aziz *et al*'s potential has been fitted to a wide range of experimental and theoretical data, and is also expected to be very accurate.

Collision integrals for the C–C interaction were taken from the tabulation given by Stallcop *et al* [53]. They performed an *ab initio* calculation based on an accurate configuration interaction method that took into account 18 potential energy curves to evaluate the collision cross-sections and collision integrals over a wide temperature range.

The HFD-B (Hartree–Fock-dispersion-B) potential of Slavíček *et al* [54] was used to evaluate the collision integrals for the Ar–Ar interaction. Slavíček *et al* fitted an *ab initio* pair intermolecular potential to a suitably chosen analytical HFD-B potential; the fitted results were found to agree very closely with experimental data for the second virial coefficients, spectral characteristics and scattering [54].

For other neutral–neutral interactions for which no accurate experimental data existed, the interaction potentials were estimated using the most accurate calculated data that could be located in the literature. For the atom–molecule and molecule–molecule interactions involving neutral carbon species, Riabov's data [55] obtained using the additive-potential method were adopted, as recommended by [56]. The

Table 1. Polarizability values of neutral species.

Species	Polarizability (Å^3)	Data source
Ar	1.641	[64]
He	0.205	[65]
C	1.780	[66]
C_2	3.200	[66]
C_3	4.900	[67]
C_4	7.512	[68]
C_5	11.164	[68]

additive-potential method was proposed by Amdur *et al* [57] for approximate calculations of interaction potentials, and can be applied with acceptable accuracy to atom–molecule and molecule–molecule interactions. The effective spherically symmetric potential corresponding to the point force centre can be determined by averaging the above-mentioned potential over equiprobable orientations. The interaction potential parameters are given by means of the exponential repulsive potential. Transport coefficients of equilibrium dissociating gases calculated from collision integrals obtained by this method have been shown to be in good agreement with experimental data [58].

Although we can note that exponential repulsive potential is not realistic at low temperatures (below approximately 2000 K) as a result of its neglect of long-range dispersion forces in the interaction potential [56], the species whose interactions are considered using this method are only present in significant quantities at low temperatures if condensed carbon is neglected in the calculation; in the real situation, the maximum mole fraction of carbon at 1 atm is under 10^{-3}. Therefore, this uncertainty has a small effect on the properties obtained here.

For the interactions between the noble atom species and neutral carbon species, an improvement of the Lennard-Jones function, i.e. a phenomenological potential developed by Capitelli and co-workers [59–61], has been used. A comparative study performed for argon has verified that the phenomenological potential models the short-range interaction more accurately, with a less-hard repulsive wall, and moreover reproduces accurate *ab initio* calculations in the long-range region very well [62]. Therefore, it can provide more accurate estimation of the interaction potential than the widely used Lennard-Jones potential when reliable experimental data or accurate theoretical calculations are unavailable.

The phenomenological potential requires polarizability values; the values used here for neutral species, and the data source, are listed in table 1.

We developed a new computer program, based on the work of Barker *et al* [63], to compute the collision integrals for the phenomenological potential.

4.2. Neutral–ion interactions

For neutral–ion interactions, two kinds of processes should be taken into account; purely elastic collisions and the inelastic resonant charge-exchange process. For l odd ($l = 1$ and 3), the latter plays an important role in determining the collision integrals $\Omega_{ij}^{(l,s)}$. Considering the elastic and inelastic processes, we follow the previous work of Murphy and Arundell [69] and estimate the total collision integrals by the empirical mixing rule:

$$\Omega^{(l,s)} = \sqrt{(\Omega_{\mathrm{in}}^{(l,s)})^2 + (\Omega_{\mathrm{el}}^{(l,s)})^2} \tag{4}$$

where the subscripts in and el denote the collision integrals derived from the inelastic and the elastic interactions, respectively.

In order to numerically evaluate the charge-exchange collision integrals, it is necessary to know the charge-exchange cross-section. For interactions between a parent atom or molecule X and its ion X^- or X^+, particularly for high energies, the transport cross-section can be evaluated using

$$Q^l(g) = 2Q_{\mathrm{ex}} \tag{5}$$

where the charge-transfer cross-section is approximated in the form

$$Q_{\mathrm{ex}} = (A - B \ln E)^2 \tag{6}$$

where E is the collision energy. The constants A and B can be obtained from experimental data or theoretical calculations.

The charge-exchange cross-section for collision between unlike species (e.g. $Y^{\pm} + X \rightarrow X^{\pm} + Y$) is small compared with the elastic collision cross-section, and is neglected in this paper. Collision integrals with even l are wholly determined by the elastic interactions.

For the Ar–Ar^+ interaction, the potential parameters for elastic collisions provided by Aubreton *et al* [70] for six molecular states of the Ar–Ar^+system were used here, as in the previous paper by Murphy and Arundell [69]. The collision integral values are in close agreement with those calculated by the Tang–Toennies effective one-dimensional potential approach, apart from a 25% discrepancy at 300 K [71]. This is of no significance because the number density of ions is negligible at such low temperatures. The inelastic collision integrals were obtained by direct integration of the charge-transfer cross-section. The constants A and B were determined by a least-squares fit to the calculated value of the charge-transfer cross-section from 0.001 to 10 eV [72], which agrees with the scarce experiment and theoretical data available in the literature.

For the He–He^+ interaction, the elastic interaction can be well described by the lower two molecular states of the He–He^+ system, i.e. $X\,^2\Sigma_u^+$ and $A\,^2\Sigma_g^+$. The potential energy curves for these electronic states were calculated by fitting accurate *ab initio* calculations with the potential models TTIA and TTIA-WB for the $X\,^2\Sigma_u^+$ and $A\,^2\Sigma_g^+$ states, respectively, based on universal damping functions for the dispersion coefficients [73]. It should be noted that the Monte Carlo simulation calculations of the He^+ ion in Heare in excellent agreement with the available experiment data in the literature (within about 5% discrepancy), indicating that the fitting interaction potential can be used in this paper with confidence. For the charge-transfer collision integral, the constants A and B were determined by a least-squares fit to the value of the charge-transfer cross-section from 0.001 to 10 eV calculated by Barata and Cond [73]. The values of A and B are in agreement with experimental data [74] within the level of uncertainty of the data.

Table 2. Polarizability values of ion species.

Species	Polarizability (Å^3)	Data source
Ar^+	1.0656	[79]
He^+	0.030	[80]
C^-	7.280	[*]
C_2^+	3.200	[*]
C^+	0.840	[*]
C^{2+}	0.368	[81]
C^{3+}	0.289	[81]
C_2^-	3.660	[*]

In the case of the C–C^+ interaction, the collision integrals for even l were calculated using the potential parameters of 16 molecular states of the C–C^+ system given by [75] in the form of the Hulburt–Hirschfelder potential [76]. We used the data presented in [67], which were estimated from the data provided in [77, 78], for the constants A and B required to determine the resonant charge-exchange cross-section.

The phenomenological potential model was adopted to represent the other interactions considered, except those involving the species Ar^{2+}, Ar^{3+} and He^{2+}. The polarizability values needed for ion species and the sources of these data are tabulated in table 2; only the ground states of these ions were considered. Unfortunately, experimental data are extremely limited for polarizabilities of some species that are present in our work. Coverage of dipole polarizabilities is particularly sparse. However, quantum chemical predictions for polarizabilities can be quite accurate if determined with a good correlated method [68]. For these species, denoted by [*] in table 2, Woon's quantum chemical prediction values of the polarizabilities by means of the finite field approach were used in this paper.

No accurate experimental data or theoretical calculations are available in the literature for the charge-exchange interactions between C and C^-. The constants A and B were determined using an empirical formula proposed by Rapp and Francis [82].

A very wide range of polarizability values are given in the literature for Ar^{2+}, Ar^{3+} and He^{2+}, which can result in large discrepancies in the collision integrals determined using the phenomenological potential model. Hence, collision integrals for interactions involving these species have been derived using a polarization potential model:

$$\varphi_{\text{in}}(r) = \left(\frac{1}{4\pi\varepsilon_0}\right)^2 \frac{(Z_{\text{i}}e)^2\alpha_{\text{n}}}{2r^4} \tag{7}$$

Z_{i} being the ion charge and α_{n} being the polarizability of the neutral species.

The collision integrals for the polarization potential were obtained by a closed form, which leads to simple relations as follows [83]:

$$\Omega_{i,n}^{(1,1)} = 424.443 Z_{\text{i}} \frac{\sqrt{\alpha_{\text{n}}}}{T}$$
$$\Omega_{i,n}^{(1,2)} = 0.833\Omega_{i,n}^{(1,1)}, \quad \Omega_{i,n}^{(2,2)} = 0.870\Omega_{i,n}^{(1,1)},$$
$$\Omega_{i,n}^{(1,3)} = 0.729\Omega_{i,n}^{(1,1)}, \quad \Omega_{i,n}^{(2,3)} = 0.761\Omega_{i,n}^{(1,1)},$$
$$\Omega_{i,n}^{(1,4)} = 0.656\Omega_{i,n}^{(1,1)}, \quad \Omega_{i,n}^{(2,4)} = 0.685\Omega_{i,n}^{(1,1)},$$
$$\Omega_{i,n}^{(1,5)} = 0.602\Omega_{i,n}^{(1,1)}, \quad \Omega_{i,n}^{(3,3)} = 0.842\Omega_{i,n}^{(1,1)}. \tag{8}$$

It should be noted that the use of this potential can bring about an underestimate of the collision integrals. However, since the interactions are between atoms and multiply ionized ions, the concentration of at least one of the species is always low, and the interactions have negligible influence on the transport properties [84].

4.3. Electron–neutral interactions

The collision integrals for interactions between electrons and neutral species are calculated as a function of temperature by straightforward integration of the $Q_1(E)$, $Q_2(E)$ and $Q_3(E)$ cross-sections as functions of electron energy, assuming a Boltzmann distribution. When $Q_2(E)$ and $Q_3(E)$ are not available, their ratios to the momentum transfer cross-section $Q_1(E)$ can be determined by numerical integration of differential elastic cross-sections (DCS), if these are available. The differential cross-sections $\mathrm{d}\sigma/\mathrm{d}\Omega$ can be numerically integrated over all scattering angles to obtain the transport cross-sections as a function of the interaction energy.

The most recent data in the literature were used here. For the e−He and e−Ar interactions, we used a comprehensive set of theoretical values for differential and momentum transfer cross-sections for elastic scattering of electrons by inert-gas atoms for energies below 1 keV that were presented in [85]. These were obtained by means of the critical analysis of, and comparison with, the most available accurate experimental and theoretical data. Because the differential cross-sections at the energy below 1 eV were not given in [85], we fixed the lowest electron energy to 0.01 eV in our calculation, and other transfer cross-sections were obtained at this energy using the relations $Q_2(E) = 2/3Q_1(E)$ and $Q_3(E) = Q_1(E)$, which are the limiting values at zero energy.

The only available DCS for the e–C interaction, those computed by Thomas and Nesbet [86] at energies between 0.1 and 7.0 eV, were adopted, with extrapolated values used at lower and higher energies. The values obtained are larger than those calculated from the theoretical data in [87].

For the e–C_2 interaction, the only available data come from theoretical studies [88]. Calculated elastic differential and momentum transfer cross-sections reported in the 0.1–1000 eV energy range were adopted to obtain the transport cross-sections $Q_1(E)$, $Q_2(E)$ and $Q_3(E)$, and extrapolated to the lowest energy, 0.01 eV, using the same approach mentioned above.

For other electron–neutral interactions, unfortunately, to our knowledge, no available experimental or calculated data are available in the literature. The cross-sections were estimated by assuming that the cross-sections are independent of energy and dominated by polarization effects [89]. These crude approximations mean that the values of electrical conductivity at low levels of ionization are not likely to be accurate [90]. However, for two reasons, these uncertainties can be neglected under the condition considered here. First, because electron–ion collision cross-sections are about three

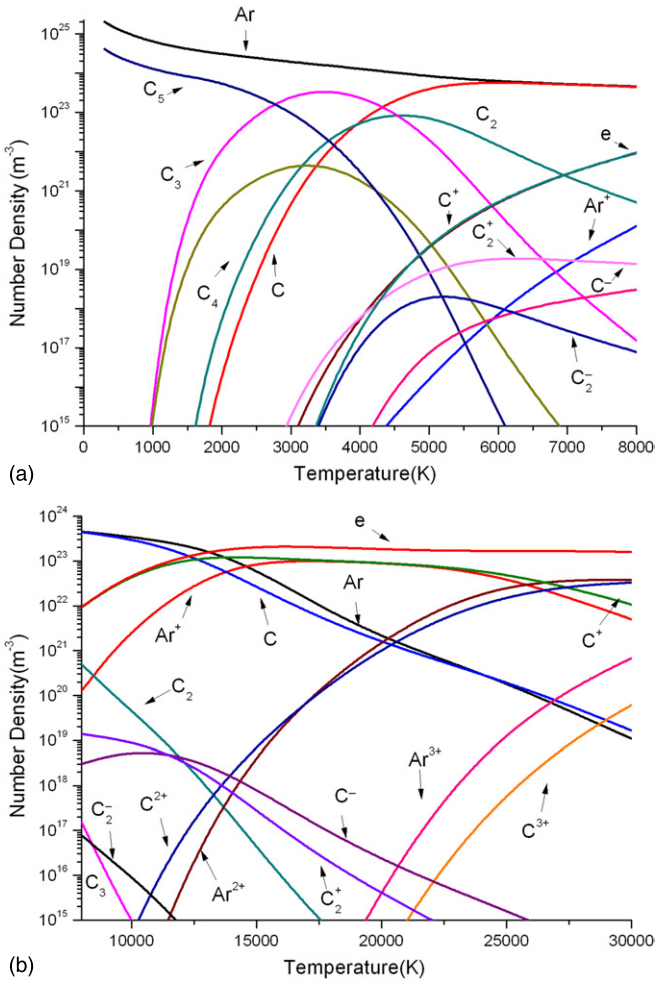

Figure 1. Temperature dependence of equilibrium composition of 50% C and 50% Ar at 1 atm, neglecting condensed carbon.

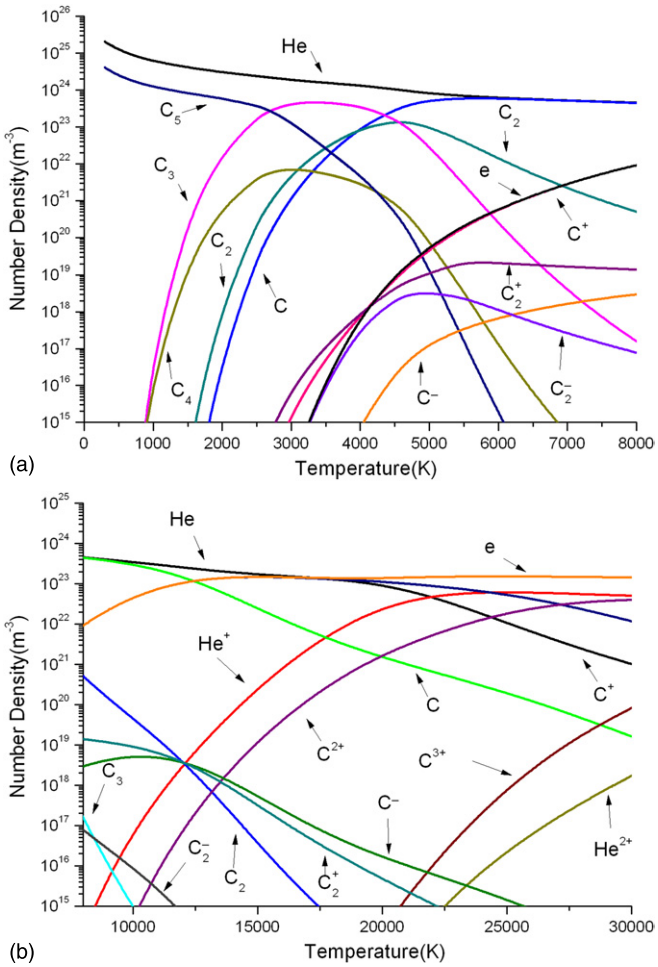

Figure 2. Temperature dependence of equilibrium composition of 50% C and 50% He at 1 atm, neglecting condensed carbon.

orders of magnitude greater than electron–neutral cross-sections, accurate values of the latter cross-sections are important only for small degrees of ionization (<1%). Second, when ionization begins, the concentrations of those species for which these estimates were adopted are extremely low, so the effect on the electrical conductivity is negligible.

4.4. Charged–charged interactions

These interactions were described by a Coulomb potential screened at the Debye length by the presence of charged particles. The effective collision integrals were calculated from the works of Mason *et al* [44, 91], where the Debye length is calculated taking into account only electrons.

5. Results and comparisons

5.1. Equilibrium composition

The equilibrium compositions of mixtures of 50% C and 50% Ar, and 50% C and 50% He, neglecting condensed carbon, are depicted in figures 1 and 2, respectively. Note that all percentages refer to volume or mole percentages. The calculations were carried out for the temperature range from 300 to 30 000 K and at atmospheric pressure. Unless specifically noted, the results are determined without taking into account the solid carbon formation.

In the temperature range from 300 to 8000 K, the following points should be noted:

(1) The concentration of C_5 (the largest carbon molecule considered) decreases as the temperature increases because of dissociation to form C_4 and C_3, whose concentrations are maximum at 3100 K and 3500 K, respectively. Further temperature increases lead to further dissociation of C_4 and C_3 to form C_2 and C.

(1) The ionization degree becomes significant (at least 10^{-6}) only above about 4000 K; at these temperatures the dominant ion is C^+. Both dissociation and ionization of molecular C_2 occur in the temperature range from 3800 to 16 000 K.

(3) The mole fractions of the species C_2^+, C_2^- and C^- are always lower than 1.0×10^{-4}, which means they may be classified as minor species. However, they are still considered in this calculation in order to obtain a more accurate result. For higher temperatures, the main carbon species are atoms and ions. Above 12 000 K, the second ionization of carbon to C^{2+} starts to become significant.

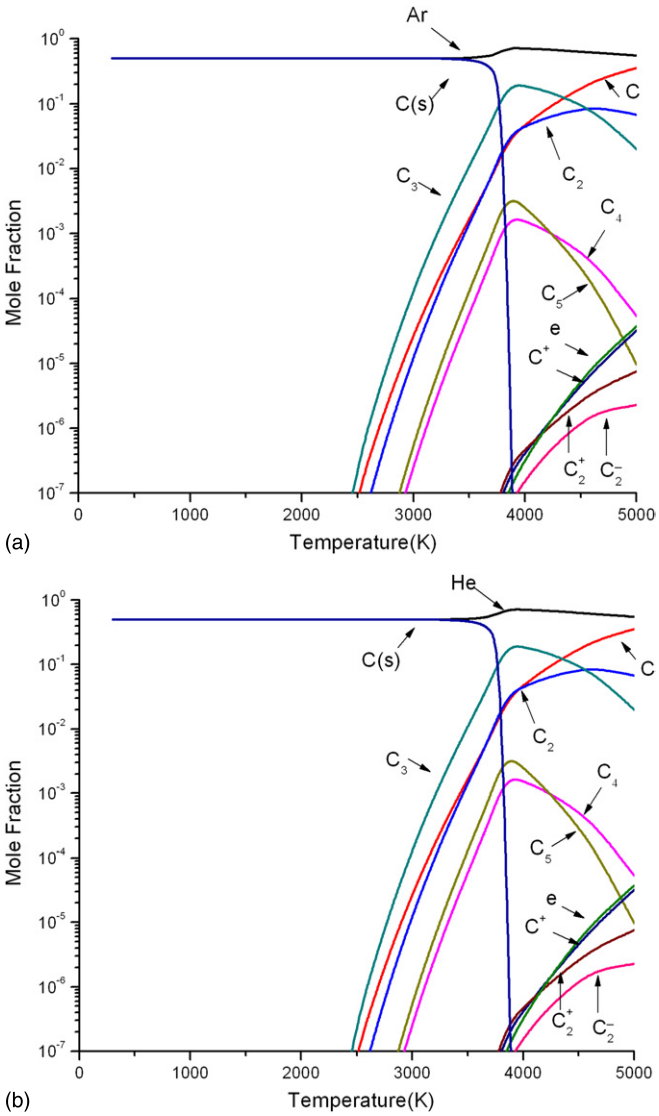

Figure 3. Influence of condensed carbon on the equilibrium composition of mixtures of 50% C and 50% Ar, and 50%C and 50% He, at 1 atm.

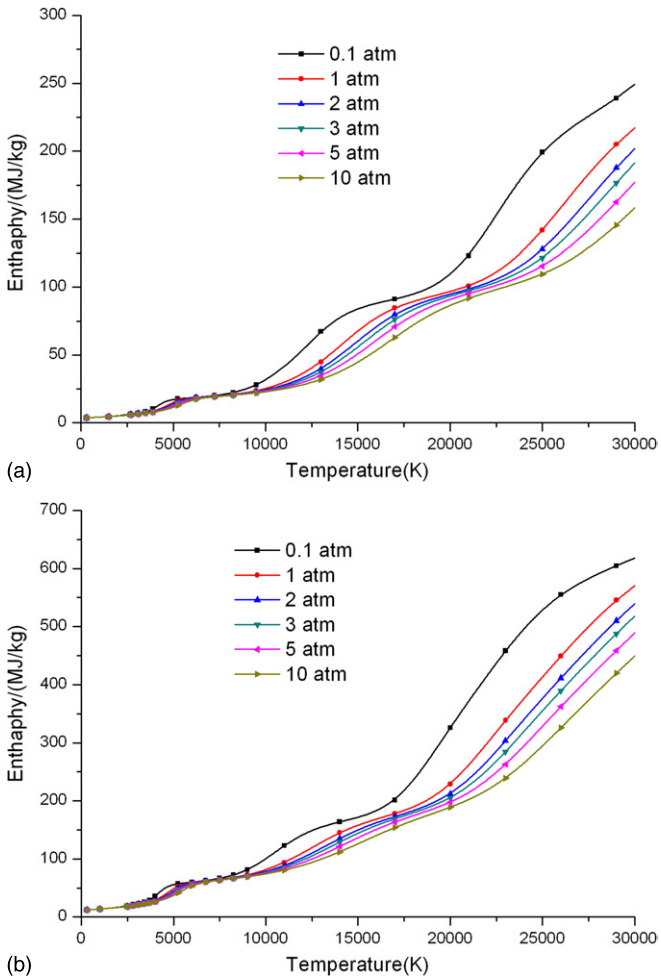

Figure 4. Temperature dependence of enthalpy of mixtures of 50% C and 50% Ar (*a*), and 50% C and 50% He (*b*) without considering solid carbon at different pressures.

(4) Argon and helium begin to ionize at higher temperatures than carbon, around 5500 K and 10 000 K, respectively, due to their larger ionization energies. As the temperature increases, the concentration of argon and helium atoms decreases monotonically because of continuing ionization. The ionization of helium starts at a higher temperature than that of carbon and argon because of its higher ionization energy. The number density of electrons reaches its maximum value at round 17 000 K decreasing slowly at higher temperatures since the increase in electron mole fraction due to occurrence of multiple ionization is more than compensated by the decrease in total number density required to keep the pressure constant.

While the gaseous phase is always present in the system, substances in the condensed state, in one or more condensed phases, may also be present and have a substantial impact on the species composition and other properties in a certain temperature range [92]. The influence of condensed carbon on the equilibrium mole fraction of 50% C and 50% Ar, and 50% C and 50% He, at 1 atm can be seen in figure 3. The equilibrium mole fractions of the main species formed in the low-temperature range (from 300 to 5000 K) are similar for the two gas mixtures because the main reactions are dissociation reactions and the ionization degree of the mixtures is low. The solid phase of carbon disappears at around 3800 K, which is the temperature of the phase transition at 1 atm. The mole fraction of the noble gas component in the system has a slight increase after the phase transition occurs, because the condensed carbon atoms form molecular gas-phase species. The condensed carbon clearly affects the composition below the temperature of phase transition; its influence on other properties will be discussed later

5.2. Thermodynamic properties

Chemical reactions contribute significantly to the specific enthalpy and specific heat at constant pressure as shown in figures 4 and 5, respectively. The influence of the mixing ratio of carbon and noble gas is shown in figures 6 and 7.

The addition of argon or helium to carbon affects the specific enthalpy strongly, as illustrated in figure 6. Below about 6000 K, the specific enthalpy of carbon vapour is higher

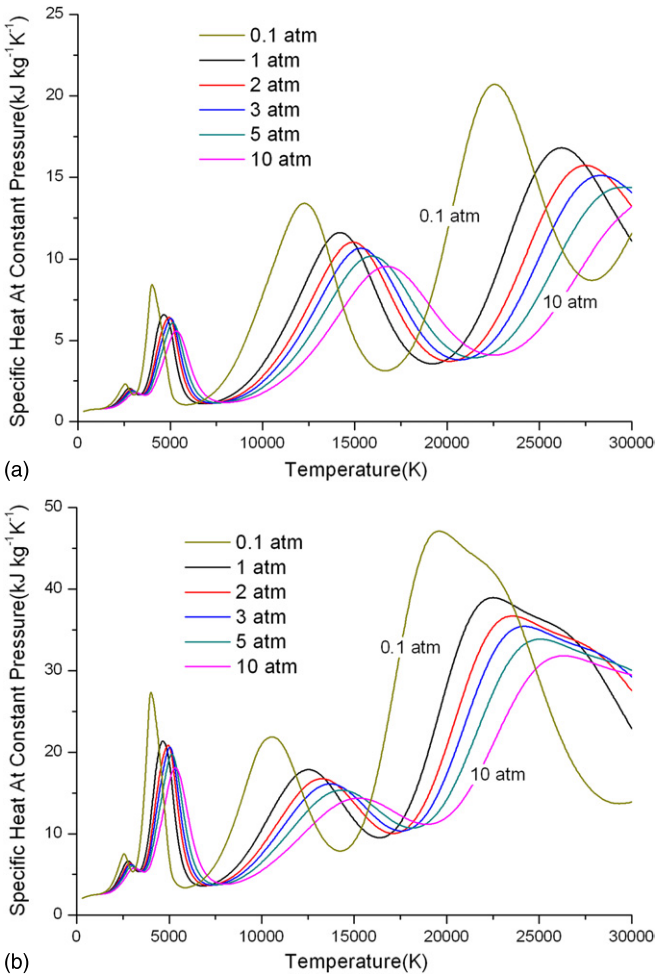

Figure 5. Temperature dependence of specific heat of 50% C and 50% Ar (*a*), and 50% C and 50% He (*b*) without considering solid carbon at different pressures.

than that of argon or helium. The ionization degree is low and there are no chemical reactions between carbon-containing species and argon or helium; therefore, increasing the concentration of argon or helium decreases the total specific enthalpy of the mixture. When ionization occurs, the influence of adding argon differs from that of adding helium, as a consequence of their different masses and ionization potentials. It is noted that the first and second ionization potentials of carbon and argon are similar, while those of helium are much greater than those of carbon. Above about 6000 K, the addition of argon to carbon decreases the specific enthalpy, mainly because of the larger mass of argon. In contrast, addition of helium decreases the specific enthalpy below about 18 000 K, and increases the enthalpy at higher temperatures. This is because the enthalpy required to ionize carbon atoms dominates at lower temperatures, and that required to ionize helium atoms dominates at higher temperatures.

The steep changes in enthalpy correspond to the peaks in the specific heat at constant pressure that originate from the heats of the dissociation and ionization reactions. Taking the carbon–argon mixture as an example, the peaks in the specific heat at constant pressure at atmospheric pressure correspond to successive dissociations of molecular carbon at around 2800 K and 4500 K, the first ionization of carbon and argon at around 12 000–15 000 K, and the second ionization of carbon and argon at around 26 000–28 000 K. It is noted that the low-temperature maxima corresponding to the carbon molecular dissociation reactions are not distinct because of their close proximity in temperature. For carbon–helium mixtures, the specific heat peak due to first ionization of helium at around 22 000 K is superimposed on the one associated with the second ionization of carbon at around 28 000 K, as demonstrated in figure 7.

As described in figure 5, when the pressure increases, the temperature at which a given peak in the specific heat occurs is increased according to Le Chatelier's law; the increase of the pressure opposes changes to the original state of equilibrium so that dissociation and ionization are suppressed, and the temperature at which these reactions occur is increased [93].

When condensed carbon is taken into account, a change of specific enthalpy and specific heat takes place due to the phase transition. This can be clearly seen in figures 6(*c*), (*d*) and 7(*c*), (*d*), which illustrate the details for specific enthalpy and specific heat of carbon–argon and carbon–helium mixtures, respectively, in the temperature range below 10 000 K. The main gas species below the transition temperature is the noble gas atom, i.e. argon and helium. As the phase transition proceeds, a larger amount of carbon reaches the gas phase in the form of molecules and atoms, as we can see from the results including solid carbon in figures 6 and 7. This changes the values of specific enthalpy and specific heat of the mixtures because of the different enthalpy and specific heat values of carbon species and noble gas atoms. The specific heat values calculated by Pousse *et al* at 100 kPa are presented for comparison, and excellent agreement is found except for a slight discrepancy in the temperature range in which carbon molecules dissociated. This is probably due to different thermodynamic data for the individual species.

5.3. Transport properties

5.3.1. Validation of the transport properties of pure noble gases. The equilibrium properties of pure argon and helium plasmas have been studied widely in the literature, since they are very important for many applications. There are few experimental measurements of transport coefficients at high temperatures, so it is important to check the consistency of our equilibrium calculations with other results. Equilibrium pure argon and helium plasmas can be regarded as benchmark systems, and are used to validate our studies by comparison with calculated and experimental results in the literature. Our results compare satisfactorily with most of the theoretical results presented by different authors [30, 69, 83, 94] as can be seen in figures 8 and 9, which display viscosity and thermal conductivity data.

For the viscosity of pure argon, excellent agreement is found with the results of Murphy and Arundell [69] and Aubreton *et al* [94], with the maximum viscosity value, which occurs at about 10 000 K differing by less than 5%.

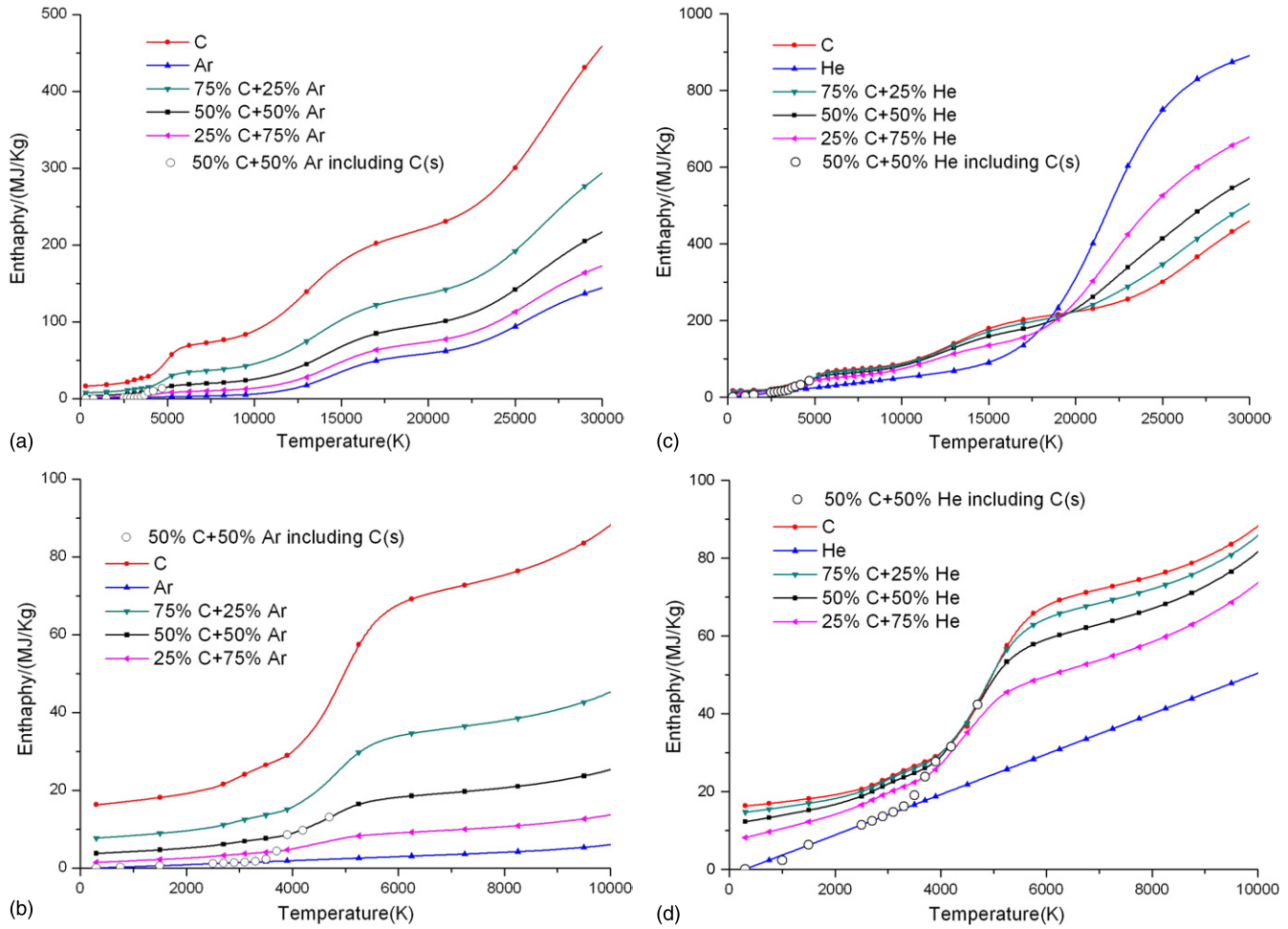

Figure 6. Temperature dependence of enthalpy of carbon–argon (*a*), (*b*) and carbon–helium (*c*), (*d*) mixtures at 1 atm for different mixing ratios.

Murphy and Arundell and Aubreton *et al* both used the same HFDTCS2 potential for the Ar–Ar interaction and the same Ar–Ar^+ interaction potential in their calculations. Our Ar–Ar pair interaction was determined using the accurate *ab initio* results of Slavíček *et al* [54], which agree with the HFDTCS2 potential to within the experimental error. For temperatures above 10 000 K, in which range Ar–Ar^+ collisions dominate, exact agreement with the results of Murphy and Arundell and Aubreton *et al* occurs because the same elastic interaction potential was used for the Ar–Ar^+ interaction.

Similar considerations apply to the viscosity of pure helium. Our results closely follow Murphy's data [30]. Although the data sources for the main interaction potentials, He–He and He–He^+, are different, they are all based on accurate *ab initio* calculations which fit the experimental data well. Differences from Bruno *et al*'s recent calculations [83] are observed, especially at temperatures above 15 000 K. Bruno *et al* took into account the shielding effect of both ions and electrons in calculating the Debye length. In the present work, only the electrons are included; this is a standard procedure that leads to a larger value of the Coulomb collision integrals [95].

As in the case of viscosity, the main deviation of total thermal conductivity for pure argon occurs at temperatures around 15 000 K, at which the reactive thermal conductivity associated with the first ionization makes an important contribution. Differences of up to 10% from the results of Murphy and Arundell [69] and Aubreton *et al* [94] arise, due to the different charge-transfer cross-section chosen for Ar–Ar^+ interaction, which dominates in this temperature range. Our charge-transfer cross-section, calculated by fitting Barata's results [72], is higher than other authors' data, which decreases the height of the peak. Note that Wright and Levin [71] have published diffusion collision integrals for Ar–Ar^+, calculated using the momentum transfer cross-section data given by Phelps [96], with which our collision integral values agree to within 3%. Our lower total thermal conductivity value is further validated by its close agreement (with relative error below 3%) with Murphy and Arundell's data [69] revised to use the Ar–Ar^+ collision integral calculated from the data of Phelps.

Our calculated dependence of pure helium thermal conductivity on temperature as well as the comparison with other recent results appearing in the literature is also given in figure 9. Our values closely follow the results of Murphy's calculation [30] except for a slight discrepancy, of less than 5%, in the maximum value. The larger discrepancy with Bruno *et al*'s data [83] can again be explained as being due to the different definition of Debye length.

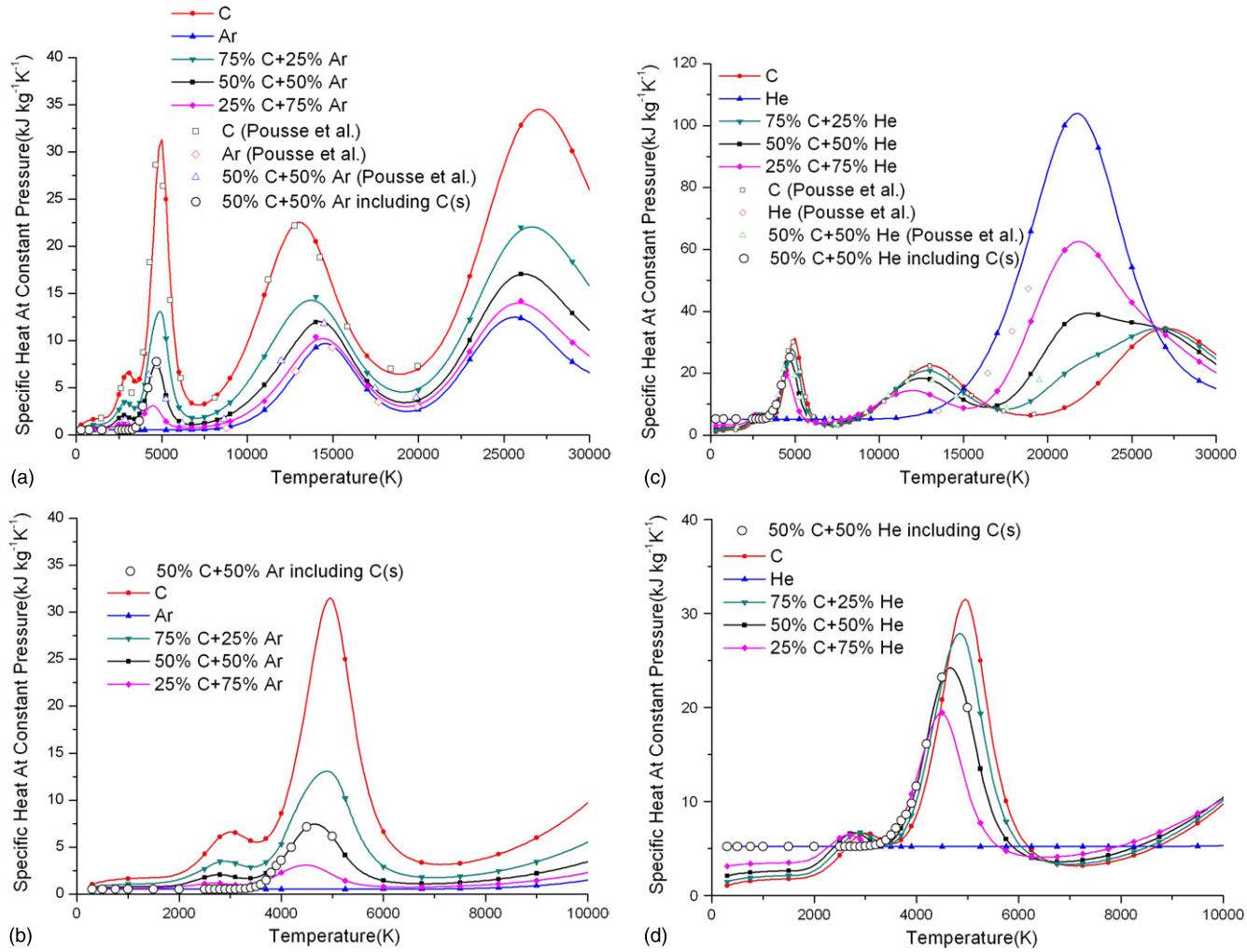

Figure 7. Temperature dependence of specific heat of carbon–argon (*a*), (*b*) and carbon–helium (*c*), (*d*) mixtures at 1 atm for different mixing ratios. Results of Pousse *et al* [31] are shown for comparison.

5.3.2. Diffusion coefficients. Because the number of the ordinary diffusion coefficients required to describe plasmas is large (one for each pair of species), only the values of the thermal diffusion coefficient of electrons are presented here. The behaviour of thermal diffusion coefficient of the electrons as a function of temperature and pressure is presented in figure 10. The influence of the mixing ratio can be seen in figure 11. The electron thermal diffusion coefficient depends appreciably on the pressure. However, the dependence is significantly reduced at lower temperatures owing to the very low concentration of electrons in the mixtures. Pure carbon and argon have almost identical values between 18 000 and 22 000 K because interactions between electrons and singly ionized ions dominate. The value is lower for helium at temperatures below 18 000 K because the degree of ionization is lower.

Solid carbon, which is present only below the ionization temperature, has negligible influence on the electron thermal diffusion coefficients, so the corresponding results are not presented here.

5.3.3. Viscosity. The dependence of viscosity on pressure and the mixing ratio of carbon and the noble gas is much more pronounced, as shown in figures 12 and 13. The viscosity increases with temperature when neutral species dominate, and decreases when significant ionization occurs as a result of the large collision integrals for the Coulomb interaction. Figure 12 indicates that the viscosity at a given temperature increases with pressure, at least at those pressures for which ionization is significant. This is because the degree of ionization decreases for increased pressure, so the Coulomb interactions become less important.

For pure carbon, a steep rise in viscosity at about 2500 to 5000 K, corresponding to the dissociation of carbon molecules, is shown in figure 13. Compared with the only available published calculation for pure carbon, that of Pousse *et al* [31], a large discrepancy exists in the temperature range from 300 to 20 000 K. This cannot be explained by the level of approximation used (the results obtained using the first and second orders of approximation of Chapman–Enskog are within 15% for these conditions), and therefore should be attributed to the different interaction potentials used in the calculations.

Pousse *et al* obtained collision integrals for the C–C interaction using a weighted average of four attractive exponential potentials and two Morse potentials. The other

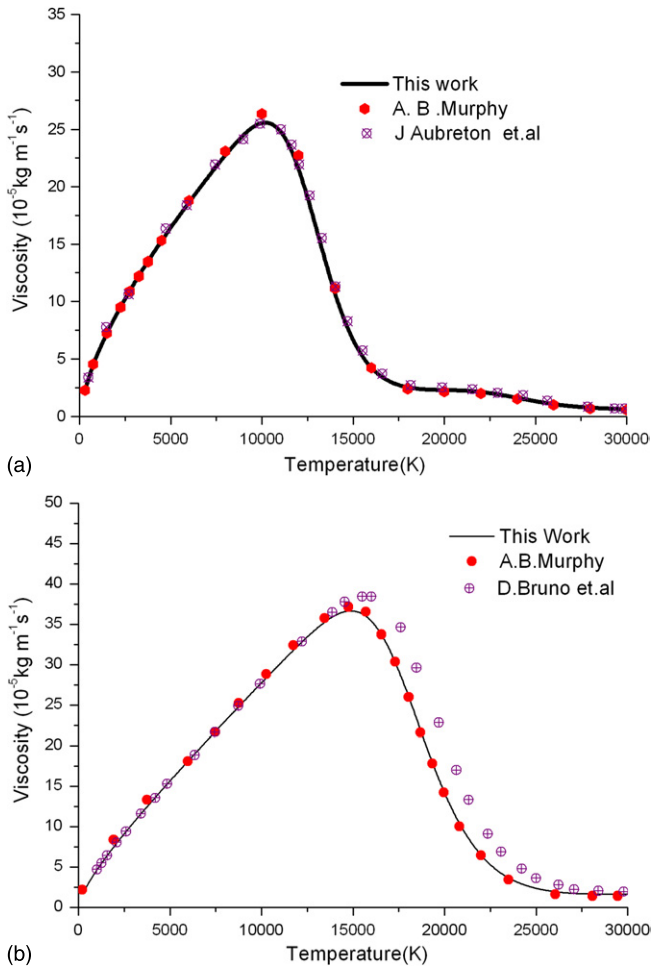

Figure 8. Temperature dependence of viscosity of argon (*a*) and helium (*b*) at 1 atm. The calculated results of Murphy and Arundell [69] and Aubreton *et al* [94] for argon, and Murphy [30] and Bruno *et al* [83] for helium are shown for comparison.

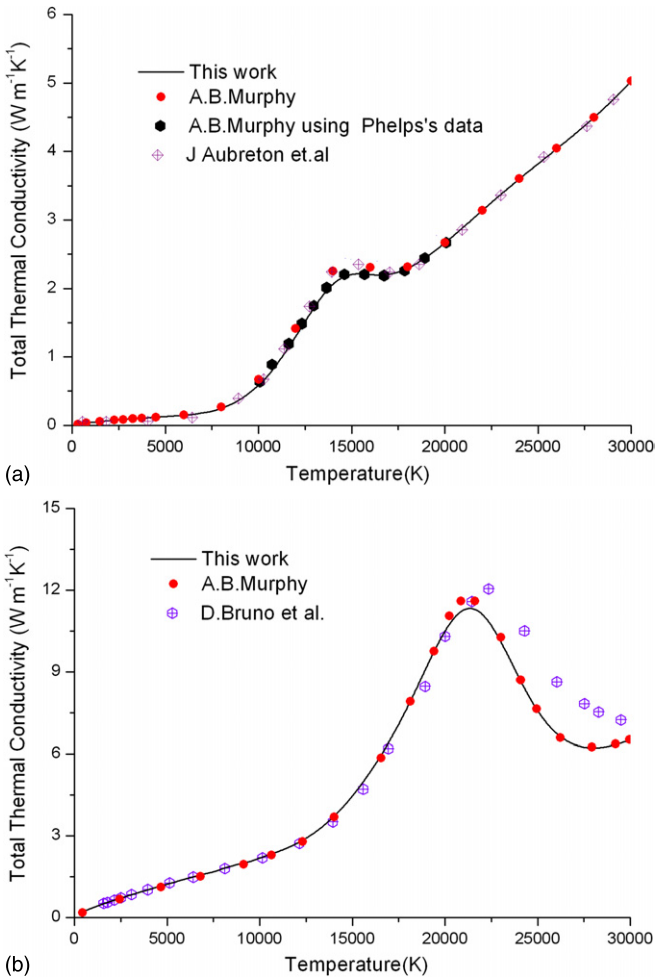

Figure 9. Temperature dependence of total thermal conductivity of argon (*a*) and helium (*b*) at 1 atm. The calculated results of Murphy and Arundell [69] with the Ar–Ar$^+$ collision integral replaced with that calculated from the data of Phelps [96], Aubreton *et al* [94] for argon, and Murphy [30] and Bruno *et al* [83] for helium are shown for comparison.

12 potential energy states of the ground state carbon atom interaction were omitted, giving rise to a large underestimate. The discrepancy is 25% at low temperatures, and increases as the temperature rises, which significantly affects the viscosity at 1 atm in the temperature range from 4000 to 9000 K in which C–C interactions dominate.

For the C–C_2 interaction, the collision integrals obtained by Pousse *et al* using an exponential attractive potential show close agreement, to within 5%, with our data. Other carbon molecular interactions, which correspond to the dissociation reactions that occur when the phase transition is neglected, dominate below temperature 4000 K. Below 2500 K, the properties are determined by the species C_5. Rough estimates based on the hard sphere model, which strongly relies on the radii of the species, have been applied in Pousse *et al*'s paper; the difference with our collision integrals contributes strongly to the deviation of the viscosity value. At temperatures above 9000 K, the discrepancy is mainly a consequence of the different collision integral values used for the C–C^+ interaction. Our data were calculated from the Hulburt–Hirschfelder potentials for the 16 available potential energy curves that were obtained by accurate *ab initio* calculations. In contrast, Pousse *et al*'s elastic collision integrals were calculated using a polarization potential, which leads to a significant underestimate.

Our results for pure argon and helium agree well with those of Pousse *et al*. They computed the collision integrals for the Ar–Ar interaction using a Morse potential, which leads to a slight deviation due to the slightly softer repulsive wall. Moreover, the collision integrals for the Ar–Ar$^+$ interaction were determined based on the same potential states, even though they were obtained from different sources. For helium, a repulsive exponential potential with a more repulsive wall at higher temperatures was used by Pousse *et al* for the He–He interaction, which gives a higher viscosity value. They used the same potential for He–He$^+$ as Murphy [30], but obtained slightly higher viscosities at high temperatures. This may be because the Debye length was calculated including electrons and ions (as was the case for Bruno *et al* [83]), but this cannot be verified since Pousse *et al* did not specify how they determined the Debye length.

The addition of a noble gas causes a drastic increase in the viscosity compared with that of pure carbon. The viscosity of

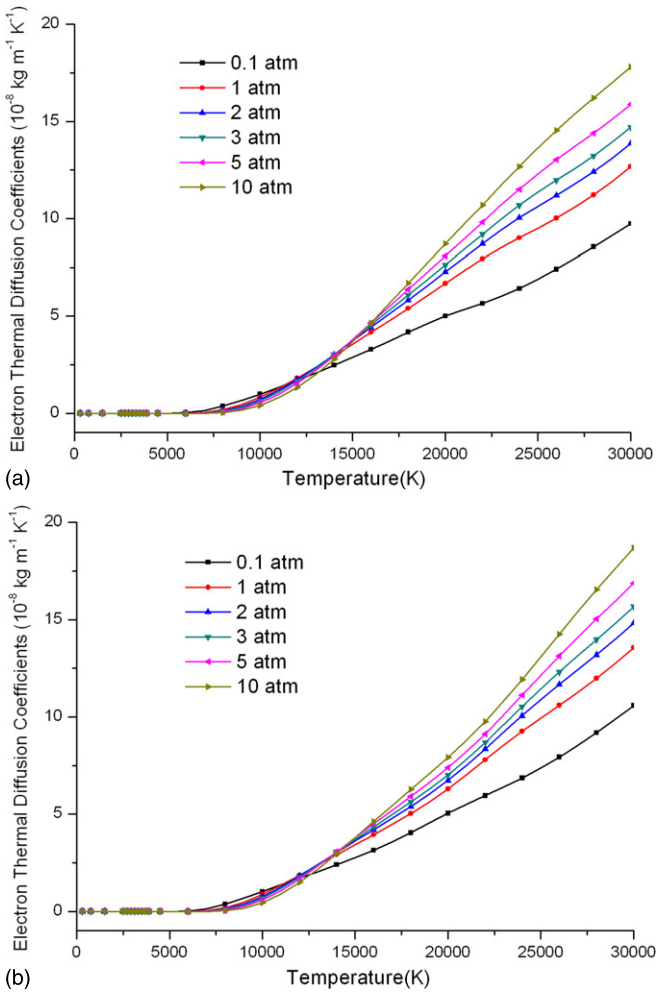

Figure 10. Temperature dependence of electron thermal diffusion coefficients of 50% C + 50% Ar (*a*) and 50% C + 50% He (*b*) without considering solid carbon, at different pressures.

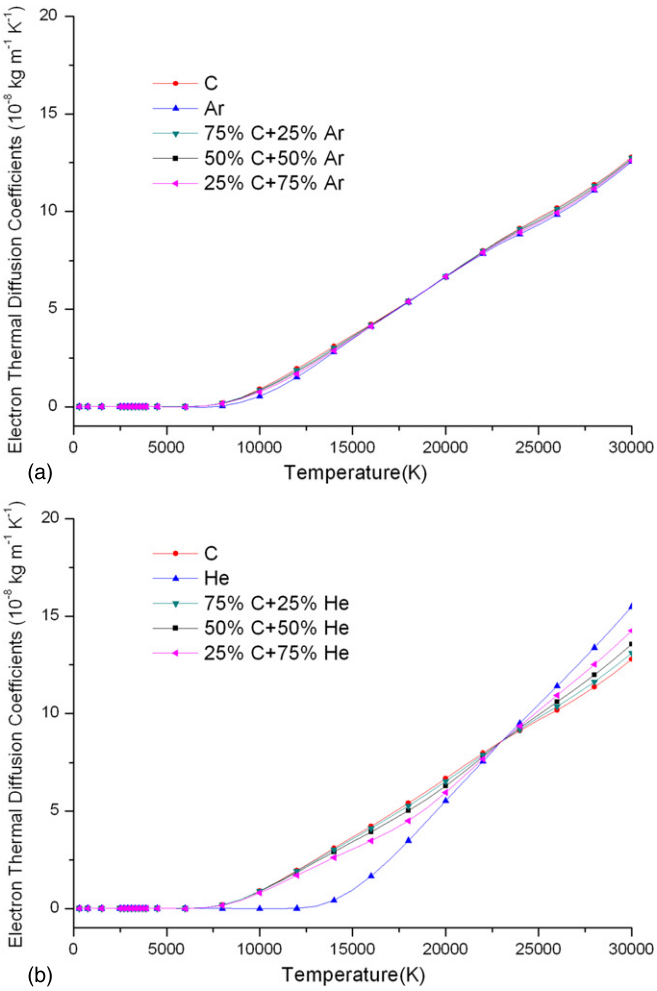

Figure 11. Temperature dependence of electron thermal diffusion coefficients of carbon–argon (*a*) and carbon–helium (*b*) mixtures at 1 atm for different mixing ratios.

the carbon–argon mixtures has a single peak at 10 000 K, since the ionization energies of the two atoms are reasonably close. The larger difference between the ionization temperatures of carbon and helium atoms leads to the appearance of double peaks in the viscosity of their mixtures for larger proportions of helium.

The height of the first peak in the viscosity of the carbon–helium mixture, which corresponds to the ionization of carbon, is higher in our results than those of Pousse *et al*. In addition to the influence of the C–C^+ and C–C interactions in this temperature range, as described above, the C–He and He–C^+ interactions also contribute to this discrepancy. The phenomenological potential used here to describe these interactions provides much more accurate collision integrals than those given by the Lennard-Jones potential and polarization potential used by Pousse *et al*, which results in a large overestimate.

The second peak of the viscosity curve corresponds to the ionization of helium atoms and C^+ ions. The large discrepancy between our viscosity values near this peak and those of Pousse *et al* can be explained by the different potentials used for the He–C^+ interaction. As shown in figure 13, if we use collision integrals for the He–C^+ interaction obtained using the polarization potential, we are able to reproduce the viscosity data of Pousse *et al* around the peak at 18 000 K. Indeed, it has been demonstrated for several ion–neutral interactions that the ratio of the viscosity and diffusion collision integrals is underestimated when the polarization potential is used [56].

The influence of condensed phase of carbon on the viscosity of 50% noble gas and 50% carbon mixtures at 1 atm pressure is also shown in figure 13. A jump corresponding to the discontinuity in composition caused by the phase transition is found.

5.3.4. Thermal conductivity. We now consider thermal conductivity, which determines the heat transfer. Figure 14 depicts the thermal conductivity of 50% carbon and 50% noble gas mixtures for the six aforementioned pressure values. As the temperature rises, the peaks that correspond to the dissociation and ionization are shifted to higher temperatures for the same reason as discussed in the case of specific heat. The temperature dependence of the thermal conductivity of mixtures of carbon and noble gas in three different proportions is compared in figure 15 with that of pure argon, pure helium and pure carbon; a comparison with the results of Pousse *et al* is also presented.

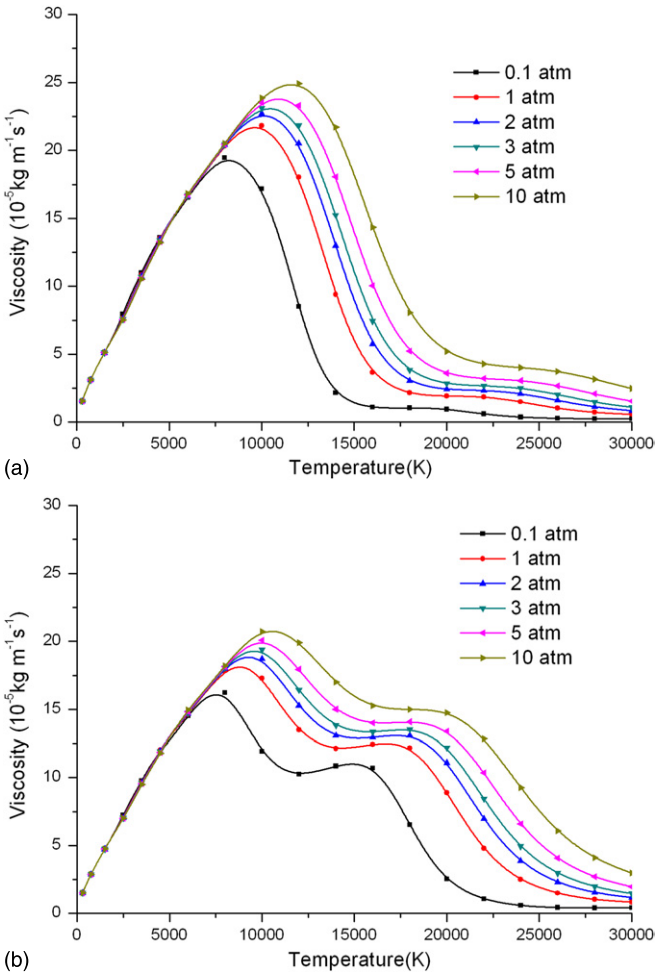

Figure 12. Temperature dependence of viscosity of 50% C + 50% Ar (*a*) and 50% C + 50% He (*b*) without considering solid carbon at different pressures.

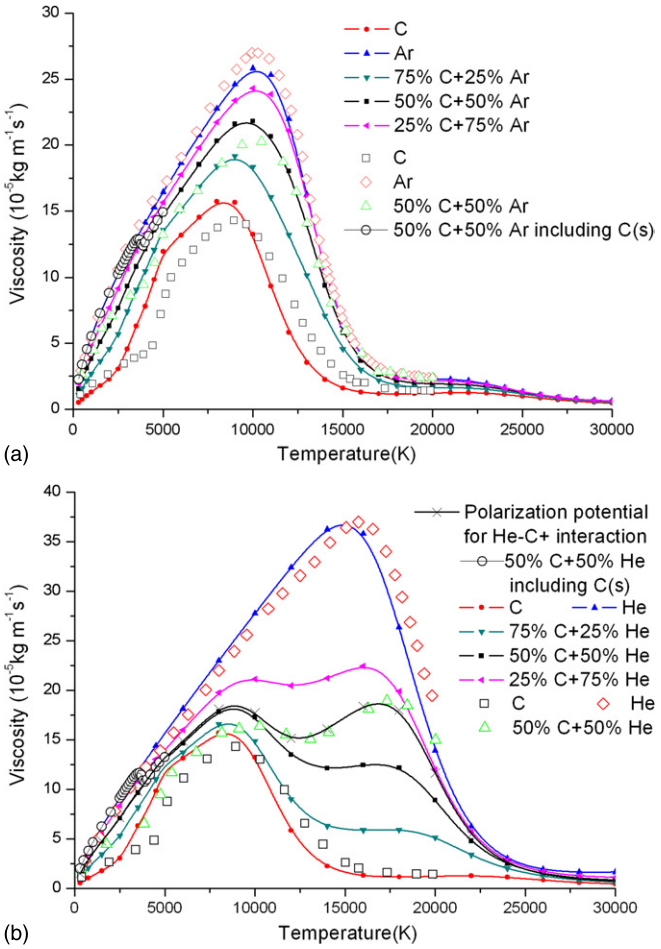

Figure 13. Temperature dependence of viscosity of carbon–argon (*a*) and carbon–helium (*b*) mixtures at 1 atm for different mixing ratios. Our results are shown using lines plus symbols, while those of Pousse *et al* [31] are shown using symbols alone.

Figure 16 shows the different components of thermal conductivity for 50% mixtures of carbon and noble gas at a pressure of 1 atm. The internal component makes a negligible contribution to the total thermal conductivity. For the carbon–argon mixture, the heavy species translational component increases slowly until around 10 000 K because the collision integrals for the interactions between neutral species decrease; after a plateau it then decreases slowly owing to the occurrence of ionization. The heavy species translational thermal conductivity plays a major role in the temperature range 6000–9000 K. The contribution of electron translation to the total thermal conductivity surpasses that of heavy species for temperatures exceeding 9000 K. Above around 14 000 K, the electron translational component dominates and heavy species' translation makes a negligible contribution. For the carbon–helium mixture, two maxima in the heavy species translational thermal conductivity occur because the first ionization reactions of carbon and helium occur at very different temperatures. The heavy species translational component has a large absolute value (>0.5 W m^{-1} K^{-1}) in a wide temperature range of 3000–21 000 K and is dominant from 6000 to 12 000 K. Above 12 000 K, the total thermal conductivity is dominated by the electron translational component.

Dissociation and ionization reactions lead to strong peaks in the thermal conductivity through the reaction thermal conductivity. For the carbon–argon mixture, the two peaks are related to the dissociation of carbon molecules, and the first ionization of carbon and argon atoms, respectively. For the carbon–helium mixture, due to the large difference of the first ionization energies, the ionization of carbon and helium atoms produce separate peaks.

Generally good agreement is found with the data of Pousse *et al* for pure argon and helium. The large discrepancies for pure carbon can be attributed to the different data sources of collision integrals that were noted in considering the viscosity above. Pousse *et al*'s underestimation of the collision integrals for the C–C$^+$ interaction is responsible for the greater height of the second peak in the thermal conductivity.

In most situations, the thermal conductivity of carbon and noble gas mixtures has values intermediate to those of the pure gases. However, an 'anomalous' behaviour, which is a departure from this trend, exists in our results, as it does in those of Pousse *et al*. In our results, this occurs in the temperature range from 10 000 to 22 000 K for carbon–argon mixtures and 3500 to 4200 K and 10 000 to 12 000 K for carbon–helium mixtures at 1 atm. The anomalous behaviour

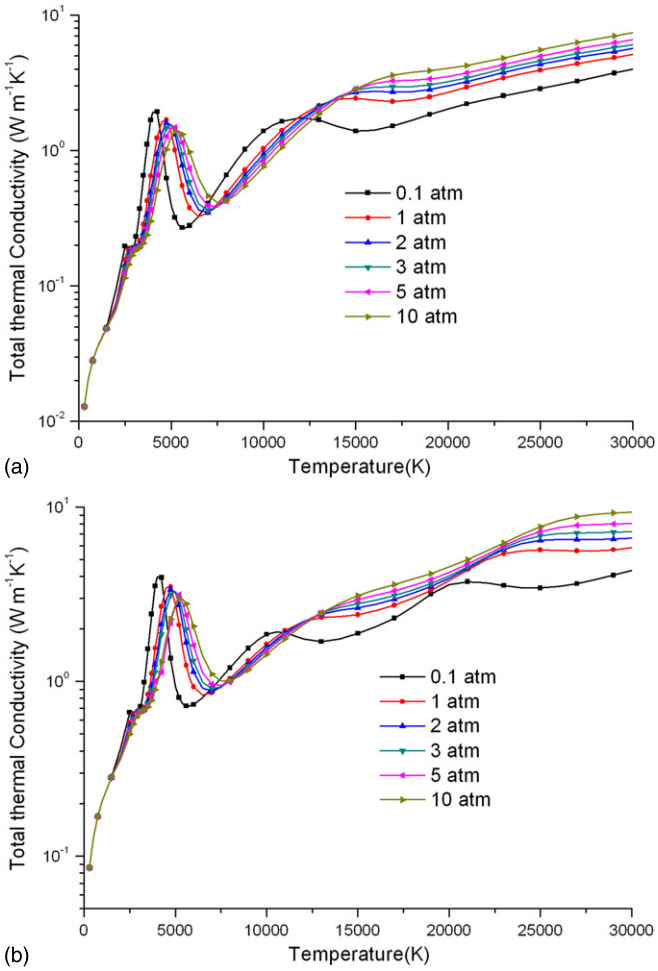

Figure 14. Temperature dependence of total thermal conductivity of 50% C + 50% Ar (*a*) and 50% C + 50% He (*b*) at different pressures.

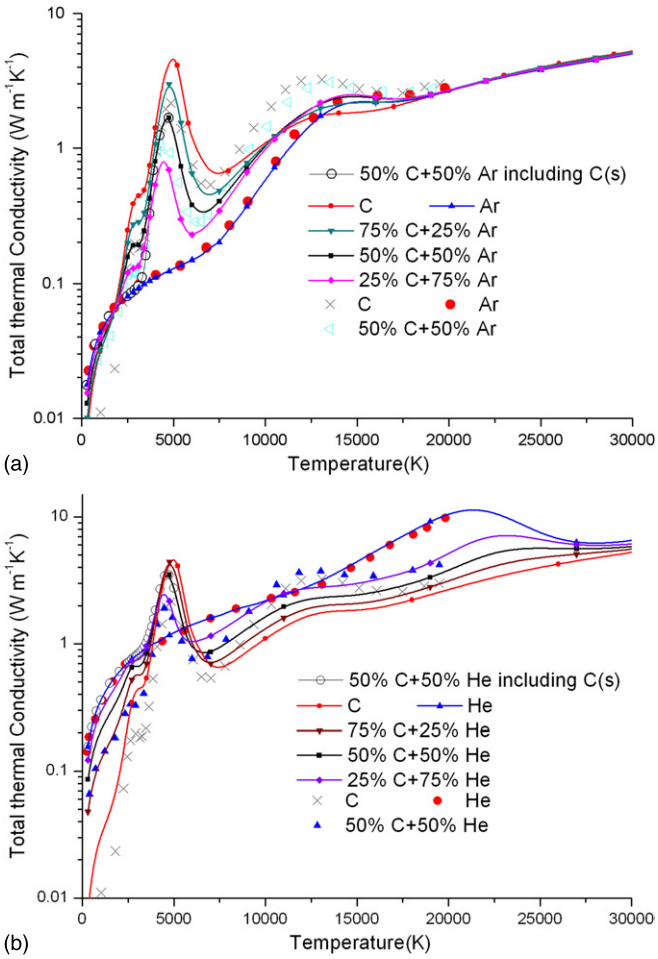

Figure 15. Temperature dependence of total thermal conductivity of carbon–argon (*a*) and carbon–helium (*b*) mixtures at 1 atm for different mixing ratios. Our results are shown using lines plus symbols, while those of Pousse *et al* [31] are shown using symbols alone.

of carbon–argon mixtures can be explained mainly by the increase in reactive thermal conductivities associated with the ionization of carbon and argon atoms in the mixtures, compared to those in pure carbon and argon. For carbon–helium mixtures, the decreasing partial pressure of carbon-containing species with the addition of helium leads to a slight shift towards lower temperatures of the dissociation peaks of carbon molecules between about 3500 to 4200 K leading to a higher thermal conductivity than that of pure carbon in this narrow temperature range. In the temperature range 10 000–12 000 K, the higher total thermal conductivity of a mixture of 25% carbon and 75% helium, compared to that of pure helium, is mainly attributable to the higher reactive and electron translational thermal conductivities as a result of the ionization of carbon atoms, which dominate the decreased heavy species translational conductivity when carbon is added to pure helium.

It is noted that for carbon–helium mixtures, the anomalous behaviour persists to a small degree in the present work, and only for mixtures with carbon below 25% mole fraction. For Pousse *et al*, the thermal conductivity of a mixture of 50% carbon and 50% helium is larger than those of pure carbon and helium in a wide temperature range, from 9500 to 14 000 K. The overestimated values are probably related to the fact that they used the polarization potential for the He–C^+ interaction in their calculation, which gave a larger translational thermal component.

Taking into account solid carbon leads to a significant change at low temperatures. The anomalous behaviour no longer exists for the carbon and helium mixture in the temperature range in which the carbon molecular dissociation takes place. Below the phase transition temperature, the thermal conductivity is determined by pure noble gas because of the negligible proportion of carbon species in the gas phase system.

5.3.5. Electrical conductivity. The electrical conductivity is directly connected to the electron density, i.e. the ionization degree of the plasma. The electrical conductivity decreases as the pressure increases at temperatures below about 11 000 K, as shown in figure 17. This is because the ionization temperature increases with pressure, so the ionization degree is lower at a given temperature. Above about 11 000 K, the electron density, and thus the electrical conductivity, increases with pressure.

From the comparison with the previous study shown in figure 18, for the pure gases our values of electrical

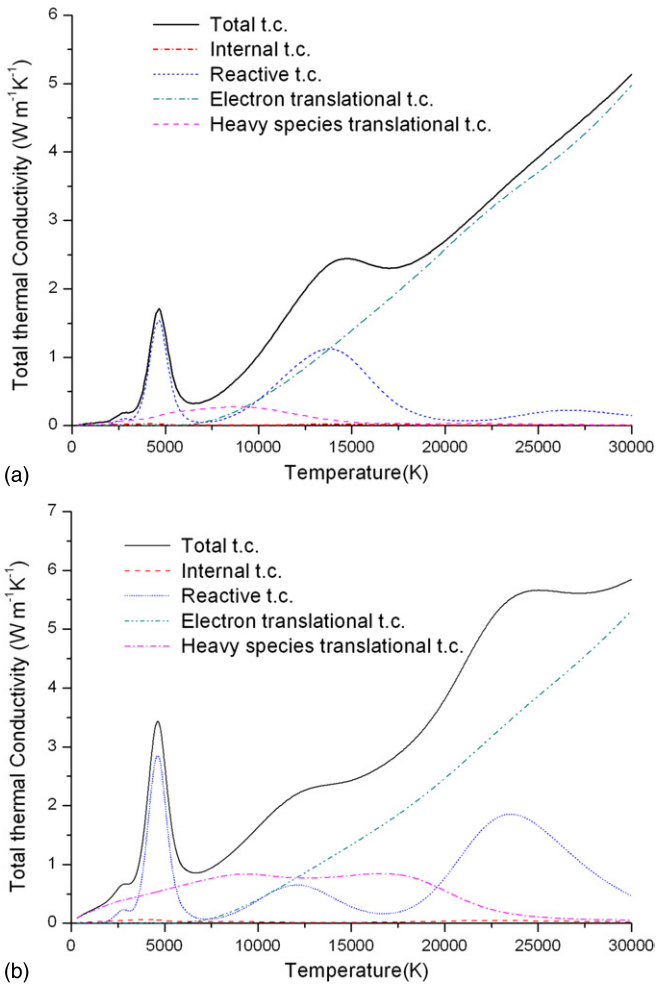

Figure 16. Temperature dependence of thermal conductivity (t.c.) components of 50% C + 50% Ar (*a*) and 50% C + 50% He (*b*) at 1 atm pressure.

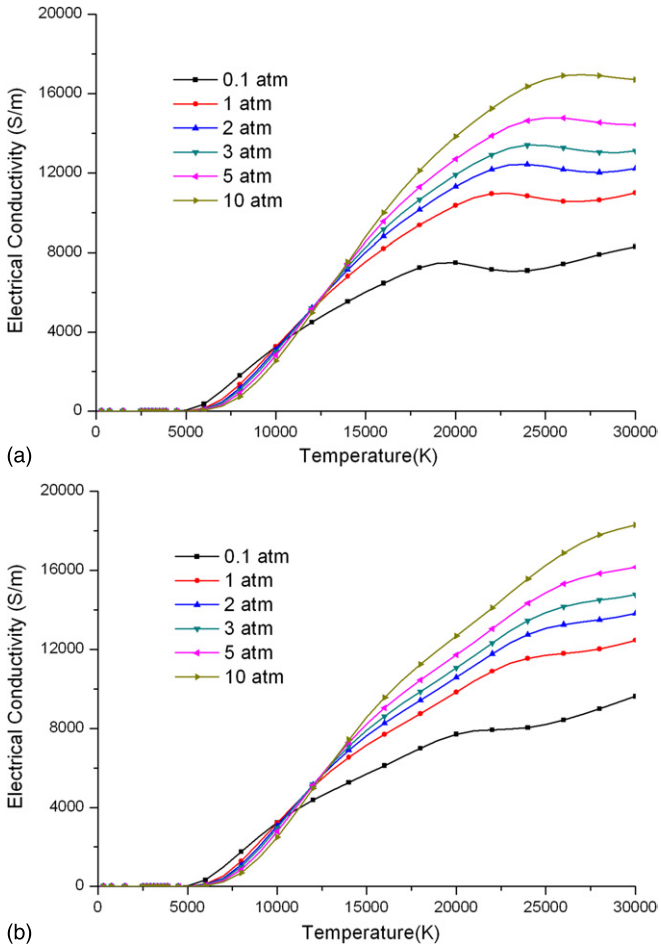

Figure 17. Temperature dependence of electrical conductivity of 50% C + 50% Ar (*a*) and 50% C + 50% (*b*) He at different pressures.

conductivity are slightly larger than those of Pousse *et al* at high temperatures. Pousse *et al* noted that their results were nearly identical to those given by Pateyron *et al* [97] and Devoto *et al* [98]. Note that the latter took into account the shielding effect of both ions and electrons in their definition of Debye length. A similar discrepancy was noted earlier in the case of viscosity.

The electrical conductivity of mixtures containing a few per cent of carbon is closer to that of pure carbon than to that of the noble gas. In the case of argon, the electrical conductivity of mixtures containing a few per cent of carbon is even higher than that of pure carbon, for temperatures below 9000 K at 1 atm pressure. This can be explained from the first approximation expression of electrical conductivity, which is

$$\sigma(1) = \frac{3e^2 n_e}{8\sqrt{2\pi k T m_e}\sum_{j\neq e}^{\nu} n_j \overline{\Omega}_{e,j}^{(1,1)}}. \qquad (9)$$

Although the electron density is slightly lower for the mixture, this is counteracted by the influence of the electron–atom collision cross-section, which is much smaller for argon atoms than for carbon atoms.

At temperatures above 22 000 K, the electrical conductivity of mixtures of carbon and argon tends to decrease due to the formation of multiply charged ions, which have higher Coulomb collision integrals, as described in figure 18, which have higher Coulomb collision integrals. In the case of helium, this decrease is shifted to higher temperatures as the proportion of carbon decreases, because the ionization of helium occurs at higher temperatures than that of carbon.

Including the carbon phase transition has negligible influence on the electrical conductivity, since significant ionization does not occur at the relevant temperatures.

6. Discussion and conclusion

In this paper, a considerable effort was devoted to the calculation of thermodynamic properties and transport coefficients of carbon–argon and carbon–helium plasmas in LTE for temperatures from 300 to 30 000 K and pressures from 0.1 to 10 atm, which are conditions relevant to a wide range of applications. The plasma composition was determined by the minimization of the Gibbs free energy, and thermodynamic properties were presented in detail. For the calculation of transport coefficients, use was made of collision integrals obtained by recent intermolecular interaction studies. A reliable database of high-order collision integrals involving all

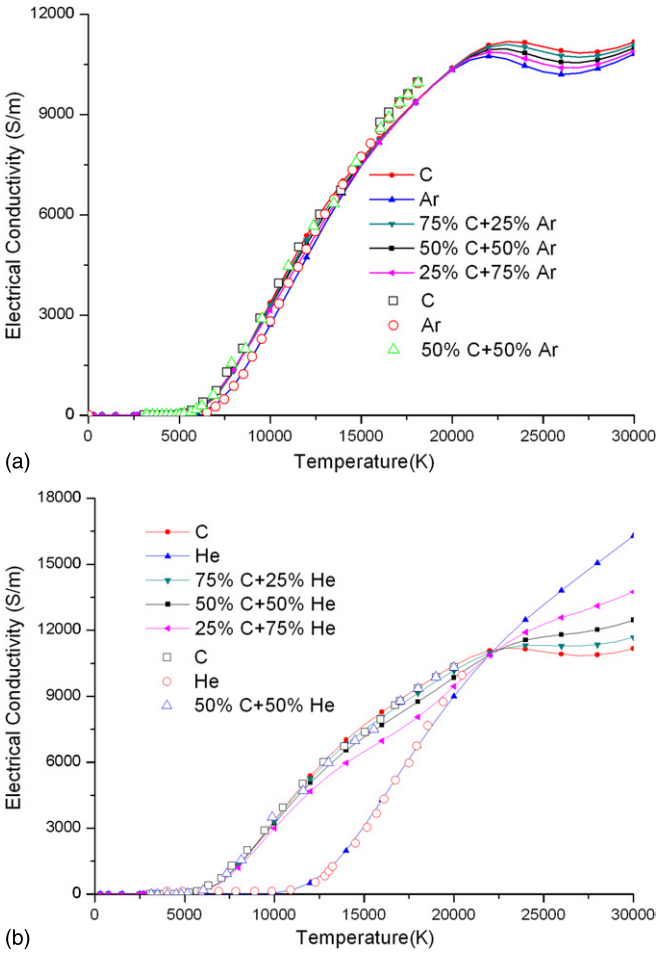

Figure 18. Temperature dependence of electrical conductivity of carbon–argon (*a*) and carbon–helium (*b*) mixtures at 1 atm for different mixing ratios. Our results are shown using lines plus symbols, while those of Pousse *et al* [31] are shown using symbols alone.

important neutral–neutral, neutral–ion, electron–neutral and charged interactions was developed. Validation of the transport coefficients determined using these collision integrals was carried out by comparing with available data in the literature. Generally good agreement was found with most data for pure argon and helium, in particular the more recent data. Some discrepancies exist between the transport coefficients obtained here for carbon and carbon–argon and carbon–helium mixtures and those presented in the literature; these can be accounted for in terms of differences in certain collision integrals used in the calculation.

A comparison of results with and without considering the formation of solid carbon shows its significant influence on the composition, and hence, thermodynamic properties and transport coefficients. As a result of the solid carbon condensation, only small amounts of carbon species appear below the phase transition temperature in the gaseous system, and hence pure gas argon or helium dominates. At the phase transition temperature, more carbon species suddenly become part of the gaseous system causing a discontinuous increase in most of the gas properties as the temperature increases through the transition temperature. Solid carbon only appears under conditions for which the ionization degree is quite low and its influence on electron-related properties, i.e. electron thermal diffusion coefficients and electrical conductivity, can be ignored.

The results presented here are expected to have a higher accuracy than those previously published, and are reliable reference data for use in the simulation of plasmas in argon, helium, carbon, and carbon–argon and carbon–helium mixtures.

Acknowledgments

This work was supported by the Chinese Government Scholarship program for postgraduates and the National Natural Science Foundation of China, No 50907047. The authors are grateful to Dr David E Woon for sending them calculated values of the polarizabilities of relevant species.

References

[1] Ostrikov K, Cvelbar U and Murphy A B 2011 Plasma nanoscience: setting directions, tackling grand challenges *J. Phys. D: Appl. Phys.* **44** 174001
[2] Kroto H W, Heath J R, O'Brien S C, Curl R F and Smalley R E 1985 C60: Buckminsterfullerene *Nature* **318** 162–3
[3] Varma C M, Zaanen J and Raghavachari K 1991 Superconductivity in the fullerenes *Science* **254** 989-92
[4] Tagmatarchis N and Shinohara H 2001 Fullerenes in medicinal chemistry and their biological applications *Mini-Rev. Med. Chem.* **1** 339–48
[5] Vincent D and Cruickshank J 1997 Optical limiting with C(60) and other fullerenes *Appl. Opt.* **36** 7794–8
[6] Oh I K, Jung J H, Jeon J H and Sridhar V 2010 Electro-chemo-mechanical characteristics of fullerene-reinforced ionic polymer–metal composite transducers *Smart Mater. Struct.* **19** 075009
[7] Zhang S F, Shearman J R, Domin M, Lazaro M J, Herod A A and Kandiyoti R 1997 Catalytic activity of fullerenes for hydrocracking coal extracts *Fuel* **76** 207–14
[8] Iijima S 1991 Helical microtubules of graphitic carbon *Nature* **354** 56–8
[9] Dravid V P, Host J J, Teng M H, Elliott B, Hwang J, Johnson D L, Mason T O and Weertman J R 1995 Controlled-size nanocapsules *Nature* **374** 602
[10] Host J J, Teng M H, Elliott B R, Hwang J H, Mason T O, Weertman J R, Johnson D L and Dravid V P 1997 Graphite encapsulated nanocrystals produced using a low carbon : metal ratio *J. Mater. Res.* **12** 1268–73
[11] Zhang M, Fang S, Zakhidov A A, Lee S B, Aliev A E, Williams C D, Atkinson K R and Baughman R H 2005 Strong, transparent, multifunctional, carbon nanotube sheets *Science* **309** 1215–9
[12] Dalton A B, Collins S, Munoz E, Razal J M, Ebron V H, Ferraris J P, Coleman J N, Kim B G and Baughman R H 2003 Super-tough carbon-nanotube fibres *Nature* **423** 703
[13] Collins P G, Arnold M S and Avouris P 2001 Engineering carbon nanotubes and nanotube circuits using electrical breakdown *Science* **292** 706–9
[14] Kordas K, Toth G, Moilanen P, Kumpumaki M, Vahakangas J, Uusimaki A, Vajtai R and Ajayan P M 2007 Chip cooling with integrated carbon nanotube micro-fin architectures *Appl. Phys. Lett.* **90** 123105
[15] Belluci S 2005 Carbon nanotubes: physics and applications *Phys. Status Solidi* c **2** 34–47

[16] Shihonara H, Sato H, Saito Y, Takayama M, Izuoka A and Sugawara T 1991 Formation and extraction of very large all-carbon fullerenes *J. Phys. Chem.* **95** 8449–51
[17] Novoselov K S, Geim A K, Morozov S V, Jiang D, Zhang Y, Dubonos S V, Grigorieva I V and Firsov A A 2004 Electric field effect in atomically thin carbon films *Science* **306** 666–9
[18] Geim A K and Novoselov K S 2007 The rise of graphene *Nature Mater.* **6** 183–91
[19] Ebbesen T W and Ajayan P M 1992 Large scale synthesis of carbon nanotubes *Nature* **358** 220–2
[20] Pulickel M A and Otto Z Z 2001 Applications of carbon nanotubes *Top. Appl. Phys.* **80** 391–425
[21] Bethune D S, Kiang C H, Devries M S, Gorman G, Savoy R, Vazquez J and Beyers R 1993 Cobalt-catalysed growth of carbon nanotubes with single-atomic-layer walls *Nature* **363** 605–7
[22] Lowell D L and Donald R H 1993 Fullerene production *J. Phys. Chem. Solids* **54** 1635–43
[23] Zhang H Y, Wang D Y and Xue X M 1997 The effect of helium gas pressure on the formation and yield of nanotubes in arc discharge *J. Phys. D: Appl. Phys.* **30** L1–4
[24] Volotskova O, Levchenko I, Shashurin A, Raitses Y, Ostrikov K and Keidar M 2010 Single-step synthesis and magnetic separation of graphene and carbon nanotubes in arc discharge plasmas *Nanoscale* **2** 2281–5
[25] Karmakar S, Kulkarni N V, Nawale A B, Lalla N P, Mishra R, Sathe V G, Bhoraskar S V and Das A K 2009 A novel approach towards selective bulk synthesis of few-layer graphenes in an electric arc *J. Phys. D: Appl. Phys.* **42** 115201
[26] Shi Z J, Lian Y F and Zhou X H 1999 Production of single-wall carbon nanotubes at high pressure *J. Phys. Chem.* B **103** 8698–701
[27] Zhou Y S ,Yu F F and He W X 2003 A new surfacing power-carbon electrode arc constrained by argon *Trans. China Weld. Inst.* **23** 63–5
[28] Kim K S, Moradian A, Mostaghimi J and Soucy G 2010 Modelling of induction plasma process for fullerene synthesis: effect of plasma gas composition and operating pressure *Plasma Chem. Plasma Process.* **30** 91–110
[29] Keidar M and Beilis I I 2009 Modelling of atmospheric-pressure anodic carbon arc producing carbon nanotubes *J. Appl. Phys.* **106** 103304
[30] Murphy A B 1997 Transport coefficients of helium and argon–helium plasmas *IEEE Trans. Plasma Sci.* **25** 809–14
[31] Pousse J, Chervy B, Bilodeau J F and Gleizes A 1996 Thermodynamic and transport properties of argon/carbon and helium/carbon mixtures in fullerene synthesis *Plasma Chem. Plasma Process.* **16** 605–34
[32] Coufal O 2007 Composition and thermodynamic properties of thermal plasma up to 50 kK *J. Phys. D: Appl. Phys.* **40** 3371–85
[33] Fauchais P, Boulos M I and Pfender E 1994 *Thermal Plasmas—Fundamentals and Applications* vol 1 (New York: Plenum)
[34] Gordon S and McBride B J 1971 Computer program for calculation of complex chemical equilibrium composition, rocket performance, incident and reflected shocks, and chapman jouguet detonations *NASA Publication* SP-273
[35] Murphy A B 2001 Thermal plasmas in gas mixtures *J. Phys. D: Appl. Phys.* **34** 151–73
[36] Kovitya P 1985 Physical properties of high-pressure plasmas of hydrogen and copper in the temperature range 5000 K to 30000 K *IEEE Trans. Plasma Sci.* **13** 587–94
[37] Moore C E 1949 *Atomic Energy Levels Circular 467* vol 1, US National Bureau of Standards, Washington, DC
[38] Moore C E 1952 *Atomic Energy Level Circular 467* vol 2, US National Bureau of Standards, Washington, DC
[39] Chase M W and Davies C A Jr 1998 *NIST-JANAF Thermochemical Tables* 4th edn (New York: American Institute of Physics for the National Institute of Standards and Technology)
[40] Hirschfelder J O, Curtis C F and Bird R B 1964 *Molecular Theory of Gases and Liquids* 2nd edn (New York: Wiley)
[41] Chapman S and Cowling T G 1970 *The Mathematical Theory of Non-Uniform Gases* 3rd edn (Cambridge: Cambridge University Press)
[42] Ferziger J H and Kaper H G 1972 *Mathematical Theory of Transport Processes in Gases* (Amsterdam: North-Holland)
[43] Rat V, André P, Aubreton J, Elchinger M F, Fauchais P and Lefort A 2002 Transport coefficients including diffusion in a two-temperature argon plasma *J. Phys. D: Appl. Phys.* **35** 981–91
[44] Devoto R S 1973 Transport coefficients of ionized argon *Phys. Fluids* **16** 616–23
[45] Devoto R S 1967 Third approximation to the viscosity of multicomponent mixtures *Phys. Fluids* **10** 2704–6
[46] Butler J N and Brokaw R S 1957 Thermal conductivity of gas mixtures in chemical equilibrium *J. Chem. Phys.* **26** 1636–43
[47] Meador W E and Stanton L D 1965 Electrical and thermal properties of plasmas *Phys. Fluids* **8** 1694–703
[48] Monchick L, Yun K S and Mason E A 1963 Formal kinetic theory of transport phenomena in polyatomic gas mixtures *J. Chem. Phys.* **39** 654–69
[49] Hirschfelder J O 1957 Heat conductivity in polyatomic or electronically excited gases *J. Chem. Phys.* **26** 282–5
[50] Hirschfelder J O 1957 *Proc. 6th Int. Symp. on Combustion (Reinhold, New York)* p 351
[51] Hurly J J and Mehl J B 2007 ^{4}He thermophysical properties: new *ab initio* calculations *J. Res. Natl Inst. Stand. Technol.* **112** 75–94
[52] Aziz R W, Janzen A R and Moldover M R 1995 *Ab initio* calculations for helium: a standard for transport property measurements *Phys. Rev. Lett* . **74** 1586–9
[53] Stallcop J R, Partridge H, Pradham A and Levin E 2000 Potential energies and collision integrals for interactions of carbon and nitrogen atoms *J. Thermophys. Heat Transfer* **14** 480–8
[54] Slavíček P, Kalus R, Paška P, Odvárková I, Hobza P and Malijevský A 2003 State-of-the-art correlated *ab initio* potential energy curves for heavy rare gas dimers Ar_2, Kr_2, Xe_2 *J. Chem. Phys.* **119** 2102–19
[55] Riabov V V 1988 Transfer coefficients of multicomponent air with sublimation products of graphite *J. Eng. Phys.* **55** 786–91
[56] Wright M J, Hwang H H and Schwenke D W 2007 Recommended collision integrals for transport property computations: II. Mars and Venus entries *AIAA J.* **45** 281–8
[57] Amdur I, Longmire M S and Mason E A 1961 Scattering of high-velocity neutral particles: XII. He–CH_4, He–CF_4, CH_4–CH, and CF_4–CF_4 interactions *J. Chem. Phys.* **35** 895–8
[58] Riabov V V 1996 Approximate calculation of transport coefficients of Earth and Mars atmospheric dissociating gases *J. Thermophys. Heat Transfer* **10** 209–16
[59] Pirani F, Alberti M, Castro A, Teixidor M M and Cappelletti D 2004 Atom–bond pairwise additive representation for intermolecular potential energy surfaces *Chem. Phys. Lett.* **394** 37–44
[60] Capitelli M, Cappelletti D, Colonna G, Gorse C, Laricchiuta A, Liuti G, Longo S and Pirani F 2007 On the possibility of using model potentials for collision integral calculations of interest for planetary atmospheres *Chem. Phys.* **338** 62–8
[61] Laricchiuta A, Colonna G, Bruno D, Celiberto R, Gorse C, Pirani F and Capitelli M 2007 Classical transport collision

integrals for a Lennard-Jones like phenomenological model potential *Chem. Phys. Lett* . **445** 133–9
[62] Lombardi A and Palazzetti F 2008 A comparison of interatomic potentials for rare gas nanoaggregates *J. Mol. Struct. (Theochem)* **852** 22–9
[63] Barker J A, Fock W and Smith F 1964 Calculation of gas transport properties and the interaction of argon atoms *Phys. Fluids* **7** 897–903
[64] Lupinetti C and Thakkar A J 2005 Polarizabilities and hyperpolarizabilities for the atoms Al, Si, P, S, Cl, and Ar: coupled cluster calculations *J. Chem. Phys.* **122** 044301
[65] Schmidt J W, Gavioso R M, May E F and Moldover M R 2007 Polarizability of helium and gas metrology *Phys. Rev. Lett.* **98** 254504
[66] Fridman A 2007 *Plasma Chemistry* (Cambridge: Cambridge University Press)
[67] André P, J Aubreton J and Clain S 2010 Transport coefficients in thermal plasma. Applications to Mars and Titan atmospheres *Eur. Phys. J.* D **57** 227–34
[68] Woon D E and Herbst E 2009 Computed dipole moments and dipole polarizabilies for neutral astromolecules *Astrophys. J. Suppl.* **185** 273–88
[69] Murphy A B and Arundell C J 1994 Transport coefficients of argon, nitrogen, oxygen, argon–nitrogen, and argon–oxygen plasmas *Plasma Chem. Plasma Process.* **14** 451–90
[70] Aubreton J, Bonnefoi C and Mexmain J M 1986 Calcul de propriétés thermodynamiques et des coefficients de transport dans un plasma Ar–O_2 en non-équilibre thermodynamique et à la pression atmosphérique *Rev. Phys. Appl. (Paris)* **21** 365–76
[71] Wright M J and Levin E 2005 Collision integrals for ion–neutral interactions of air and argon *J. Thermophys. Heat Transfer* **19** 127–8
[72] Barata J A S 2007 Integral and differential elastic collision cross-sections for low-energy Ar+ ions with neutral Ar atoms *Nucl. Instrum. Methods Phys. Res.* A **580** 14–7
[73] Barata J A S and Cond C A N 2010 Elastic He^+ on He collision cross-sections and Monte Carlo calculation of the transport coefficients of He^+ ions in gaseous helium *Nucl. Instrum. Methods Phys. Res.* A **619** 21–3
[74] Rundel R D, Nitz D E, Smith K A, Geis M W and Stebbings R F 1979 Resonant charge transfer in He^+–He collisions studied with the merging-beams technique *Phys. Rev.* A **19** 33–42
[75] Sourd B, Aubreton J, Elchinger M F, Labrot M and Michon U 2006 High temperatures transport coefficients in e/C/H/N/O mixture *J. Phys. D: Appl. Phys.* **39** 1105–19
[76] Rainwater J C, Holland P M and Biolsi L 1982 Binary collisions dynamics and numerical evaluation of dilute gas transport properties for potentials with multiple extrema *J. Chem. Phys.* **77** 434–47
[77] Belyaev V A, Brezhnev B G and Erastov E M 1968 Resonant charge transfer of low energy carbon and nitrogen ions *Sov. Phys.—JETP* **27** 924
[78] Asinovsky E I, Kirillin A V, Pakhomonov E P and Shabashov V I 1971 Experimental investigation of transport properties of low-temperature plasma by means of electric arc *Int. Proc. IEEE* **59** 592–601
[79] Meier P, Sandemant R J and Andrews M 1974 The static polarizability of argon ions *J. Phys. B: At. Mol. Phys.* **7** L339–41
[80] Miller T and Bederson B 1977 *Advances in Atomic and Molecular Physics* vol 13, ed D R Bates and B Bederson (New York: Academic) pp 1–55
[81] Laricchiuta A *et al* 2009 High temperature Mars atmosphere: I. Transport cross section *Eur. Phys. J.* D **54** 607–12
[82] Rapp D and Francis W E 1962 Charge-exchange between gaseous ions and atoms *J. Chem. Phys.* **37** 2631–45
[83] Bruno D *et al* 2010 Transport properties of high-temperature Jupiter atmosphere components *Phys. Plasmas* **17** 112315
[84] Murphy A B 1995 Transport coefficients of air, argon–air, nitrogen–air, and oxygen–air plasmas *Plasma Chem. Plasma Process.* **15** 279–90
[85] Mehrdad A and Constantine E T 2005 Elastic electron scattering from inert-gas atoms *At. Data Nucl. Data Tables* **91** 8–76
[86] Thomas L D and Nesbet R K 1975 Low-energy electron scattering by atomic carbon *Phys. Rev.* A **12** 2378–82
[87] Robinson E J and Geltman S 1967 Single-and double-quantum photo detachment of negative ions *Phys. Rev.* **153** 4–8
[88] Michelin S E, Oliveira H L and Soares L S S 2005 Cross sections for electron–C_2 collisions *Chem. Phys.* **309** 177–82
[89] Spencer F E and Phelps A V 1976 Momentum transfer cross sections and conductivity integrals for gases of MHD interest *Proc.15th Symp. on Engineering Aspects of MHD (Univ. of Pennsylvania, Philadelphia, PA)* p IX.9.1
[90] Kovitya P 1984 Thermodynamic and transport properties of ablated vapors of PTFE, alumina, Perspex and PVC in the temperature range 5000–30000 K *IEEE Trans. Plasma Sci.* **12** 38–42
[91] Mason E A and Munn R J 1967 Transport coefficients of ionized gases *Phys. Fluids* **10** 1827–32
[92] Coufal O and Živný O 2011 Composition and thermodynamic properties of thermal plasma with condensed phase *Eur. Phys. J.* D **61** 131–51
[93] Tanaka Y, Yamachi N, Matsumoto S, Kaneko S, Okabe S and Shibuya M 2008 Thermodynamic and transport properties of CO_2, CO_2–O_2, and CO_2–H_2 mixtures at temperatures of 300 to 30000 K and pressures of 0.1 to 10 MPa *Electr. Eng. Japan* **163** 18–29
[94] Aubreton J, Elchinger M F, Rat V and Fauchais P 2004 Two-temperature transport coefficients in argon–helium thermal plasmas *J. Phys. D: Appl. Phys.* **37** 34–41
[95] Murphy A B 2000 Transport coefficients of hydrogen and argon–hydrogen plasmas *Plasma Chem. Plasma Process.* **20** 279–97
[96] Phelps A V 1991 Cross sections and swarm coefficients for nitrogen ions and neutrals in N_2 and argon ions and neutrals in Ar for energies from 0.1 eV to 10 keV *J. Phys. Chem. Ref. Data* **20** 557–74
[97] Pateyron B, Elchinger M F, Delluc G and Fauchais P 1992 Thermodynamic and transport properties of Ar–H_2 and Ar–He plasma gases used for spraying at atmospheric pressure: I. Properties of the mixtures *Plasma Chem. Plasma Process.* **12** 421–48
[98] Devoto R S and Li C P 1968 Transport coefficients of partially ionized helium *J. Plasma Phys.* **2** 17–32